

Effects of Targeting Moiety, Linker, Bifunctional Chelator, and Molecular Charge on Biological Properties of ^{64}Cu -Labeled Triphenylphosphonium Cations

Young-Seung Kim,[†] Chang-Tong Yang,[†] Jianjun Wang,[†] Lijun Wang,[†] Zi-Bo Li,[‡] Xiaoyuan Chen,[‡] and Shuang Liu^{*†}

School of Health Sciences, Purdue University, West Lafayette, Indiana, and Molecular Imaging Program at Stanford, Department of Radiology & Bio-X, Stanford University, Stanford, California

Received December 3, 2007

In this report, we present the synthesis and evaluation of six new ^{64}Cu -labeled triphenylphosphonium (TPP) cations. Biodistribution studies were performed using the athymic nude mice bearing U87MG human glioma xenografts to explore the impact of TPP moieties, linkers, bifunctional chelators (BFCs), and molecular charge on biological properties of ^{64}Cu radiotracers. On the basis of the results from this study, it is concluded that (1) mTPP (tris(4-methoxyphenyl)phosphonium) is a better mitochondrion-targeting molecule than TPP and 3mTPP (tris(2,4,6-trimethoxyphenyl)phosphonium); (2) DO3A (1,4,7,10-tetraazacyclododecane-4,7,10-triacetic acid) and DO2A (1,4,7,10-tetraazacyclododecane-4,7-diacetic acid) are suitable BFCs for the ^{64}Cu -labeling of TPP cations; (3) NOTA-Bn (*S*-2-(4-thioureidobenzyl)-1,4,7-triazacyclononane-1,4,7-triacetic acid) has a significant adverse effect on the radiotracer tumor uptake and tumor-to-background ratios; and (4) monoanionic BFCs should be avoided to ensure that ^{64}Cu chelate has a neutral or negative charge. Considering the tumor uptake and tumor/liver ratios, $^{64}\text{Cu}(\text{DO2A-xy-TPP})^+$ is the best candidate for more extensive evaluations in different tumor-bearing animal models.

Introduction

Alteration in the mitochondrial potential ($\Delta\Psi_m$) is an important characteristic of cancer and is caused directly by mitochondrial dysfunction, such as DNA mutation and oxidative stress.^{1–4} It has been demonstrated that the mitochondrial transmembrane potential in carcinoma cells is significantly higher than that in normal epithelial cells.^{5–9} For example, the difference in $\Delta\Psi_m$ between the CX-1 colon carcinoma cell line and the control green monkey kidney epithelial cell line CV-1 was approximately 60 mV (163 mV in tumor cells versus 104 mV in normal cells). The observation that the enhanced mitochondrial potential is prevalent in tumor cell phenotype provides the conceptual basis for the development of mitochondrion-targeting pharmaceuticals and imaging probes.^{1–3,10–13}

Since plasma and mitochondrial transmembrane potentials are negative, cationic molecules with appropriate structural features can be driven electrophoretically through these membranes and accumulate inside the energized mitochondria of tumor cells.^{1–4,11} Lipophilic organic cations, such as rhodamine-123 and ^3H -tetraphenylphosphonium (^3H -TPP), have been used to measure mitochondrial potentials in tumor cells.^{1,14–16} Cationic radiotracers, such as $^{99\text{m}}\text{Tc}$ -sestamibi and $^{99\text{m}}\text{Tc}$ -tetrofosmin, are also able to localize in tumor cells due to the increased negative mitochondrial potential. $^{99\text{m}}\text{Tc}$ -Sestamibi and $^{99\text{m}}\text{Tc}$ -Tetrofosmin have been clinically used for imaging tumors of different origin and the transport function of multidrug resistance P-glycoprotein (MDR Pgp) by single photon emission computed tomography (SPECT).^{17–31} However, their cancer diagnostic values are often limited due to their insufficient tumor localization and high uptake in the heart, liver, and muscle, which makes it difficult to detect small lesions in the chest and abdominal regions. Radiolabeled triphenylphosphonium (TPP) cations, such as 4-(^{18}F -benzyl)triphenylphosphonium (^{18}F -BzTPP), have been

proposed as radiotracers for both myocardial perfusion imaging and tumor imaging by positron emission tomography (PET).^{32–38} It has been reported that ^3H -tetraphenylphosphonium (^3H -TPP) had a better tumor uptake than $^{99\text{m}}\text{Tc}$ -sestamibi, but its tumor selectivity is very poor with the tumor/heart ratio $\ll 1.0$.^{32,36,37} The high uptake of ^{18}F -BzTPP in the heart and liver may impose a significant challenge for early detection of small tumors in the chest and abdominal regions. Thus, there is an urgent need for new radiotracers that have very high tumor selectivity and high sensitivity to the changes in mitochondrial potentials at the early stage of tumor growth.

Previously, we reported the synthesis and biological evaluation of $^{64}\text{Cu}(\text{DO3A-xy-TPP})^a$, $^{64}\text{Cu}(\text{DO3A-xy-TPA})$, and $^{64}\text{Cu}(\text{DO3A-xy-mTPP})$ as PET radiotracers for tumor imaging using athymic nude mice bearing subcutaneous U87MG human glioma xenografts.³⁹ The biodistribution data clearly show that $^{64}\text{Cu}(\text{DO3A-xy-TPP})$, $^{64}\text{Cu}(\text{DO3A-xy-TPA})$, and $^{64}\text{Cu}(\text{DO3A-xy-mTPP})$ have relatively high tumor uptake with a long retention. The most striking difference between $^{64}\text{Cu}(\text{DO3A-xy-TPP})$, $^{64}\text{Cu}(\text{DO3A-xy-TPA})$, $^{64}\text{Cu}(\text{DO3A-xy-mTPP})$, and $^{99\text{m}}\text{Tc}$ -Sestamibi is that all three ^{64}Cu radiotracers have much lower heart uptake ($< 0.6\%$ ID/g) than $^{99\text{m}}\text{Tc}$ -sestamibi ($\sim 18\%$ ID/g) at > 30 min postinjection (p.i.). Their tumor/heart ratios are > 40 times

^a Abbreviations: DO3A-xy-TPP, triphenyl(4-((4,7,10-tris(carboxymethyl)-1,4,7,10-tetraazacyclododecan-1-yl)methyl)benzyl)phosphonium; DO3A-xy-TPA, triphenyl(4-((4,7,10-tris(carboxymethyl)-1,4,7,10-tetraazacyclododecan-1-yl)methyl)benzyl)arsonium; DO3A-xy-mTPP, tris(4-methoxyphenyl)-4-((4,7,10-tris(carboxymethyl)-1,4,7,10-tetraazacyclododecan-1-yl)methyl)benzyl)phosphonium; DO3A-bu-TPP, triphenyl(4-((4,7,10-tris(carboxymethyl)-1,4,7,10-tetraazacyclododecan-1-yl)methyl)-4-butyl)phosphonium; DO3A-PEG₂-TPP, triphenyl(2-(2-(2-(4,7,10-tris(carboxymethyl)-1,4,7,10-tetraazacyclododecan-1-yl)ethoxy)ethoxy)ethyl)phosphonium; DO3A-xy-3mTPP, tris(2,4,6-trimethoxyphenyl)-4-((4,7,10-tris(carboxymethyl)-1,4,7,10-tetraazacyclododecan-1-yl)methyl)benzyl)phosphonium; DO2A-xy-TPP, 4-((4,10-bis(carboxymethyl)-1,4,7,10-tetraazacyclododecan-1-yl)methyl)benzyl)triphenylphosphonium; DO2A-xy-TPP)₂, (4,4'-(4,10-bis(carboxymethyl)-1,4,7,10-tetraazacyclododecane-1,7-diyl)bis(methylene)bis(4,1-phenylene))-bis(methylene)bis(triphenylphosphonium); NOTA-Bn-xy-TPP, triphenyl(4-((3-(4-((1,4,7-tris(carboxymethyl)-1,4,7-triazonan-2-yl)methyl)phenyl)thioureido)methyl)benzyl)phosphonium.

* To whom correspondence should be addressed. Phone: 765-494-0236. Fax: 765-496-1377. E-mail: lius@pharmacy.purdue.edu.

[†] Purdue University.

[‡] Stanford University.

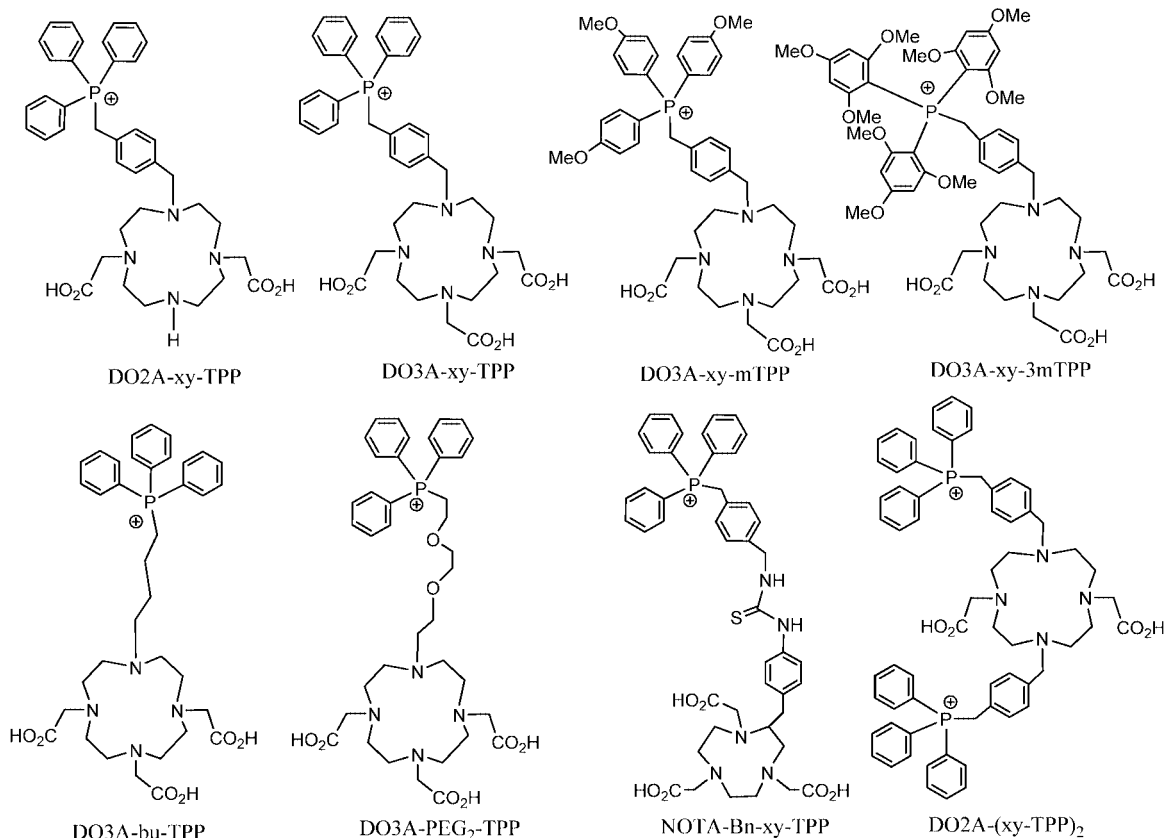


Figure 1. TPP conjugates for preparation of the ^{64}Cu -labeled TPP cations useful as tumor-selective PET radiotracers. The TPP moiety is used as the “mitochondrion-targeting biomolecule” to carry ^{64}Cu into tumor cells with higher mitochondrial potential than normal cells. DO3A, DO2A, and NOTA are used as BFCs for ^{64}Cu chelation. Different linkers are used to modify pharmacokinetics and improve tumor-to-background ratios of ^{64}Cu radiotracers.

better than that of $^{99\text{mTc}}$ -sestamibi at 120 min p.i. The muscle uptake of $^{64}\text{Cu}(\text{DO3A-xy-TPP})$, $^{64}\text{Cu}(\text{DO3A-xy-TPA})$, and $^{64}\text{Cu}(\text{DO3A-xy-mTPP})$ is almost undetectable at >30 min p.i. In contrast, $^{99\text{mTc}}$ -sestamibi has a very high muscle uptake (~5% ID/g) over a 2 h study period. Results from in vitro assays show that $^{64}\text{Cu}(\text{DO3A-xy-TPP})$ is able to localize in the mitochondria of glioma cells.³⁹ The tumor could be visualized as early as 30 min p.i. by PET imaging of the tumor-bearing mice administered with $^{64}\text{Cu}(\text{DO3A-xy-TPP})$. While the tumor uptake of the ^{64}Cu -labeled TPP cations is most likely due to the enhanced negative mitochondrial potentials, their high tumor selectivity has been attributed to their high hydrophilicity (log $P < -2.5$). It was concluded that the ^{64}Cu -labeled TPP cations are very promising PET radiotracers that are sensitive to mitochondrial potential differences between tumor cells and cells in the normal organ. However, their high liver uptake remains a significant challenge for them to be clinically useful as PET radiotracers for tumor imaging.

To improve the tumor/liver ratios of the ^{64}Cu -labeled TPP cations, we prepared ^{64}Cu complexes with several new TPP conjugates (Figure 1). Biodistribution studies were performed using athymic nude mice bearing subcutaneous U87MG glioma xenografts to explore the impact of TPP moieties, linkers, bifunctional chelators (BFCs), and molecular charge on biological properties of the ^{64}Cu -labeled TPP cations. We are particularly interested in their excretion kinetics from noncancerous organs, such as heart, liver and muscle. The U87MG human glioma cell line was chosen because it has no MDR1 Pgp expression.^{40–43} This tumor-bearing animal model would allow us to evaluate the tumor uptake of the ^{64}Cu -labeled TPP cations without complications from the MDR Pgp transport function

of tumor cells. The main objective of this study is to determine the ideal structural parameters for an optimal ^{64}Cu radiotracer that is sensitive to the early mitochondrial potential changes in tumors of different origin.

Experimental Section

Materials and Instruments. Chemicals were purchased from Aldrich (St. Louis, MO). DO3A(OBu- t_3) (1,4,7,10-tetraazacyclododecane-4,7,10-tris(*tert*-butyl acetate)), DO2A(OBu- t_2) (1,4,7,10-tetraazacyclododecane-4,7-bis(*tert*-butyl acetate)), DOTA(OBu- t_3 -NHS) (1,4,7,10-tetraazacyclododecane-1-(*N*-hydroxysuccinimide acetate)-4,7,10-tris(*tert*-butyl acetate)), and *p*-SCN-Bn-NOTA (*S*-2-(4-isothiocyanatobenzyl)-1,4,7-triazacyclononane-1,4,7-triacetic acid) were purchased from Macrocylics Inc. (Dallas, TX). NMR (^1H , ^{13}C , and ^{31}P) data were obtained using a Bruker DRX 300 MHz FT NMR spectrometer. Chemical shifts are reported as δ in ppm relative to TMS. Mass spectral data were collected using positive mode on a Finnigan LCQ classic mass spectrometer, School of Pharmacy, Purdue University. Elemental analysis was performed by Dr. H. Daniel Lee using a Perkin-Elmer Series III analyzer, Department of Chemistry, Purdue University. Cardiolite vials were obtained as a gift from Bristol Myers Squibb Medical Imaging (North Billerica, MA) and were reconstituted according to the manufacturer’s package insert. ^{64}Cu was produced using a CS-15 biomedical cyclotron at Washington University School of Medicine by the $^{64}\text{Ni}(p,n)^{64}\text{Cu}$ nuclear reaction.

HPLC Methods. Method 1 used a LabAlliance HPLC system equipped with a UV/vis detector ($\lambda = 254$ nm) and Zorbax C₁₈ semipreparative column (9.4 mm \times 250 mm, 100 Å pore size). The flow rate was 2.5 mL/min. The mobile phase was isocratic with 90% solvent A (0.1% acetic acid in water) and 10% solvent B (0.1% acetic acid in acetonitrile) at 0–5 min, followed by a gradient mobile phase going from 90% solvent A and 10% solvent

B at 5 min to 60% solvent A and 40% solvent B at 20 min. Method 2 used the LabAlliance HPLC system equipped with a UV/vis detector ($\lambda = 254$ nm), a β -ram IN-US detector, and Vydac C₁₈ column (4.6 mm \times 250 mm, 300 Å pore size). The flow rate was 1 mL/min with the mobile phase being isocratic with 90% solvent A (10 mM ammonium acetate) and 90% solvent B (acetonitrile) at 0–5 min, followed by a gradient mobile phase going from 10% B at 5 min to 60% B at 20 min.

Triphenyl(4-((4,7,10-tris(carboxymethyl)-1,4,7,10-tetraazacyclododecan-1-yl)methyl)-4-butyl)phosphonium Acetate (DO3A-bu-TPP). To a solution containing DO3A(OBu-t)₃ (52.0 mg, 0.1 mmol) and (4-bromobutyl)triphenylphosphonium bromide (47.8 mg, 0.1 mmol) and in anhydrous DMF (3 mL) was added triethylamine (0.04 mL, 0.3 mmol). The reaction mixture was stirred at room temperature for 24 h. After removal of volatiles, the residue was dissolved in 12 N HCl (3 mL). After stirring at room temperature for 10–20 min, volatiles were removed under reduced pressure. The residue was dissolved in 4 mL of a 50% DMF/water mixture, and the product was subjected to HPLC purification (method 1). Fractions at \sim 16.5 min were collected. The collected fractions were combined and lyophilized to give a white powder. The yield was 35 mg (53%). The retention time was \sim 16.5 min with the HPLC purity >95%. ¹H NMR (in D₂O): 1.66 (m, 4H), 2.78–3.51 (m, 24H), 7.55–7.67 (m, 15H, aromatic). ES-MS: $m/z = 663.76$ for [M + H]⁺ (calcd 664 for [C₃₆H₄₈N₄O₆P]⁺). Anal. Calcd for C₃₆H₄₈N₄O₆P·CH₃CO₂·H₂O: C, 61.61; H, 7.21; N, 7.56. Found: C, 61.15; H, 7.43; N, 7.35.

2,2'-(Ethane-1,2-diylbis(oxy))bis(ethane-2,1-diyl)bis(4-methylbenzenesulfonate) (TsO-PEG₂-OTs). To a solution of 4-methylbenzene-1-sulfonyl chloride (8.4 g, 44.0 mmol) and HO-(CH₂CH₂O)₃H (3.0 g, 20.0 mmol, 2.67 mL) in dichloromethane (20 mL) was slowly added triethylamine (5.1 g, 50.0 mmol). The resulting mixture was stirred at room temperature for 6 h and then heated and refluxed for another 2 h. The suspension was cooled to room temperature. After removal of the solid by filtration, the filtrate was washed by water (3 \times 20 mL). Volatiles were removed, and the light yellow solid was dissolved in dichloromethane (5 mL). Upon addition of diethyl ether (25 mL), a white solid was formed. The solid was collected by filtration and was dried under vacuum overnight to give the expected product: TsO-PEG₂-OTs. The yield was 3.7 g (40%). ¹H NMR (in CDCl₃): 2.44 (s, 6H, OCH₃), 3.52 (s, 4H), 3.65 (t, 4H, $J = 4.8$ Hz), 4.14 (t, 4H, $J = 4.8$ Hz), 7.34 (d, 4H, $J = 8.1$ Hz), 7.79 (d, 4H, $J = 8.1$ Hz). ¹³C NMR (in CDCl₃): 21.63, 68.69, 69.22, 70.65, 127.93, 129.86, 132.87, 144.88.

Triphenyl(2-(2-(2-(tosyloxy)ethoxy)ethoxy)ethyl)phosphonium Tosylate (TPP-PEG₂-OTs). To a hot toluene solution (5 mL) containing TsO-PEG₂-OTs (459.0 mg, 1.0 mmol) was added dropwise triphenylphosphine (262.0 mg, 1.0 mmol) in toluene (10 mL). The resulting mixture was then refluxed for 18 h to get a light yellow solution. Volatiles were removed under vacuum. The residue was dissolved in 50% DMF/H₂O and was subject to HPLC purification (method 1). The fractions at \sim 15 min were collected, combined, and lyophilized to give a white solid. The yield was 103.0 mg (15%). ¹H NMR (in CDCl₃): 2.25 (s, 3H, CH₃), 2.39 (s, 3H, CH₃), 3.02–3.95 (m, 12H), 7.00 (d, 2H, $J = 7.8$ Hz), 7.29 (d, 2H, $J = 8.1$ Hz), 7.53–7.78 (m, 19H). ³¹P NMR: 26.15 (s). ES-MS: $m/z = 549.12$ for [M + H]⁺ (calcd 549 for [C₃₁H₃₄O₃PS]⁺).

Triphenyl(2-(2-(2-(4,7,10-tris(carboxymethyl)-1,4,7,10-tetraazacyclododecan-1-yl)ethoxy)ethoxy)ethyl)phosphonium Acetate (DO3A-PEG₂-TPP). To a solution containing TPP-PEG₂-OTs (103.0 mg, 0.14 mmol) and DO3A(OBu-t)₃ (73.5 mg, 0.14 mmol) in anhydrous DMF (5 mL) was added triethylamine (145.0 mg, 1.43 mmol). The solution was kept at \sim 60 °C for 3 h. After removal of volatiles, the residue was dissolved in 12 N HCl (3 mL). The resulting solution was stirred at room temperature for 2 h. Volatiles were removed under reduced pressure. The residue was dissolved in 50% DMF/H₂O (3 mL) and purified by HPLC. Fractions at \sim 14.3 min were collected. The collected fractions were combined and lyophilized to give a pale yellow solid (31 mg, 28%). ¹H NMR (in D₂O): 2.72–3.79 (m, 34H), 7.47–7.72 (m, 15H). ³¹P NMR: 26.65 (s). ES-MS: $m/z = 723.20$ for [M + H]⁺ (calcd 723 for

[C₃₈H₅₂N₄O₈P]⁺). Anal. Calcd for C₃₈H₅₂N₄O₈P·CH₃CO₂·H₂O: C, 61.14; H, 7.07; N, 7.71. Found: C, 61.15; H, 7.63; N, 7.45.

4-Bromomethylbenzyl(tris-2,4,6-methoxyphenyl)phosphonium Bromide (3mTPP-xy-Br). Tris(2,4,6-trimethoxyphenyl)phosphine (1.10 g, 2.0 mmol) in toluene (6 mL) was added dropwise to a hot toluene solution (5 mL) containing α,α' -dibromo-*p*-xylene (0.53 g, 2.0 mmol). The resulting reaction mixture was refluxed at 100 °C overnight. The white solid was filtered, washed with toluene (5 mL) and ether (20 mL), and then dried under vacuum to give the product: 3mTPP-xy-Br. The yield was 1.16 g (73%). ¹H NMR (in CDCl₃): 3.59 (s, 18H, 2,6-OCH₃); 3.83 (s, 9H, 4-OCH₃); 4.55 (d, 2H, PCH₂, $J_{PH} = 15$ Hz); 4.92 (s, 2H, CH₂Br), 6.03 (s, 6H, C₆H₂); 6.91–7.05 (m, 4H, C₆H₄). ES-MS: $m/z = 715.2$ for [M⁺ + H] (calcd 715 for [C₃₅H₄₁O₉PBr]⁺).

Tris(2,4,6-trimethoxyphenyl)(4-((4,7,10-tris(carboxymethyl)-1,4,7,10-tetraazacyclododecan-1-yl)methyl)benzyl)phosphonium Acetate (DO3A-xy-3mTPP). To a solution containing 3mTPP-xy-Br (80.0 mg, 0.1 mmol) and DO3A(OBu-t)₃ (52.0 mg, 0.1 mmol) in 3 mL of anhydrous DMF was added triethylamine (0.07 mL, 0.5 mmol). The reaction mixture was stirred at room temperature overnight. After removal of volatiles under vacuum, the residue was dissolved in 2.2 mL of HCl solution (37%). After stirring at room temperature for 10–20 min, volatiles were removed under the reduced pressure. The residue was dissolved in 50% DMF/H₂O (3 mL), and the product was purified by HPLC (method 1). Fractions at \sim 23.8 min were collected. The collected fractions were combined and lyophilized to give a white powder. The yield was 40.1 mg (41%). The HPLC retention time was \sim 23.8 min with a purity of >95%. ¹H NMR (in D₂O): 2.66–3.47 (m, 22H and 2H, NCH₂); 3.51 (s, 18H, 2,6-OCH₃); 3.73 (s, 9H, 4-OCH₃); 4.63 (d, 2H, PCH₂, $J_{PH} = 13$ Hz); 6.09 (s, 6H, C₆H₂); 7.08 (d, 2H, C₆H₄); 7.19 (d, 2H, C₆H₄). ES-MS: $m/z = 981.20$ for [M + H]⁺ (calcd 981 for [C₄₉H₆₆N₄O₁₅P]⁺). Anal. Calcd for C₄₉H₆₆N₄O₁₅P·CH₃CO₂·H₂O: C, 57.84; H, 7.76; N, 7.29. Found: C, 58.15; H, 7.63; N, 7.45.

(4-((4,10-Bis(carboxymethyl)-1,4,7,10-tetraazacyclododecan-1-yl)methyl)benzyl)triphenylphosphonium Acetate (DO2A-xy-TPP). TPP-xy-Br was prepared using the procedure described in a previous report.³⁹ To a solution of TPP-xy-Br (52.6 mg, 0.1 mmol) and DO2A(OBu-t)₂ (40 mg, 0.1 mmol) in anhydrous DMF (3 mL) was added triethylamine (0.07 mL, 0.5 mmol). The reaction mixture was stirred at room temperature overnight. Volatiles were removed under vacuum, and the residue was dissolved in 2.2 mL of HCl (37%). After stirring at room temperature for \sim 15 min, volatiles were removed completely. The residue was dissolved in 4 mL of 50% DMF/H₂O (3 mL). The product was subjected to HPLC purification (method 1). Fractions at \sim 13.9 min were collected, and the collected fractions were combined and lyophilized to give a white powder. The yield was 33.0 mg (50.5%). The retention time was \sim 13.9 min with an HPLC purity of >95%. ¹H NMR (in D₂O): 2.73–3.17 (m, 21H); 4.15 (s, 2H, NCH₂); 4.68 (d, 2H, PCH₂, $J_{PH} = 13$ Hz); 6.92 (d, 2H, C₆H₄); 7.18 (d, 2H, C₆H₄); 7.43–7.76 (m, 15H, C₆H₅). ES-MS: $m/z = 653.77$ for [M + H]⁺ (654 calcd for C₃₈H₄₆N₄O₄P). Anal. Calcd for C₃₈H₄₆N₄O₄P·CH₃CO₂·3.5H₂O: C, 61.92; H, 7.28; N, 7.22. Found: C, 62.01; H, 7.18; N, 7.35.

(4,4'-(4,10-Bis(carboxymethyl)-1,4,7,10-tetraazacyclododecane-1,7-diyl)bis(methylene)bis(4,1-phenylene)bis(methylene)bis(triphenylphosphonium) Bisacetate (DO2A-(xy-TPP)₂). DO2A-(xy-TPP)₂ was isolated from the same reaction mixture as for DO2A-xy-TPP by collecting fractions at \sim 17.0 min. The collected fractions were combined and lyophilized to give a white powder. The yield for DO2A-(xy-TPP)₂²⁺ was 38.3 mg (37.6%). The retention time was \sim 17.0 min with an HPLC purity of >95%. ¹H NMR (in D₂O): 2.75–3.23 (m, 20H); 4.20 (s, 4H, NCH₂); 4.67 (d, 4H, PCH₂, $J_{PH} = 13$ Hz); 6.91 (d, 4H, C₆H₄); 7.18 (d, 4H, C₆H₄); 7.37–7.76 (m, 30H, C₆H₅). ES-MS: $m/z = 1018.79$ for [M + H]⁺ (1019 calcd for C₆₄H₆₈N₄O₆P₂); $m/z = 1039.92$ for [M + Na]⁺ (1041 calcd for C₆₄H₆₇N₄O₆P₂Na). Anal. Calcd for C₆₄H₆₈N₄O₆P₂·2CH₃CO₂·6H₂O: C, 65.58; H, 6.96; N, 4.50. Found: C, 65.03; H, 6.53; N, 4.66.

4-Aminomethylbenzyltris(phenyl)phosphonium Bromide (TPP-xy-NH₂). Phthalimide potassium (204.0 mg, 1.1 mmol) and TPP-xy-Br (526.0 mg, 1.0 mmol) were mixed in acetonitrile (20 mL). The suspension was heated to reflux for 22 h. After filtration, volatiles in the filtrate were removed under vacuum. The yellow residue was dissolved in dichloromethane (100 mL) and washed by water (30 mL). The organic phase was separated and dried over anhydrous MgSO₄. After removal of volatiles, the residue was recrystallized in the MeOH/ether mixture to give a light yellow solid (260.0 mg, 44%). ¹H NMR (in CDCl₃): 4.75 (s, 2H, CH₂N), 5.38 (d, 2H, PCH₂, J_{PH} = 14.4 Hz), 7.05 (dd, 2H, J = 8.1, 2.1 Hz), 7.14 (d, 2H, J = 8.1 Hz), 7.58–7.88 (m, 19H). The intermediate product (260.0 mg, 0.44 mmol) and 0.53 mL of aqueous hydrazine (55%, 8.8 mmol) were added into ethanol (20 mL). The resulting solution was refluxed for 20 h. Volatiles were removed under vacuum to get a light yellow solid, which was then dissolved in dichloromethane. Water was used to extract the product, and the water phase was dried under vacuum to give the expected product, TPP-xy-NH₂, as a yellow oil (120 mg, 59.0%). ¹H NMR (in CDCl₃): 3.79 (s, 2H, CH₂N), 4.63 (br s, 2H, NH₂), 5.20 (d, 2H, PCH₂, J_{PH} = 14.4 Hz), 6.94 (dd, 2H, J = 7.8, 1.8 Hz), 7.06 (d, 2H, J = 7.8 Hz), 7.56–7.68 (m, 15H).

Triphenyl(4-((3-(4-((1,4,7-tris(carboxymethyl)-1,4,7-triazonan-2-yl)methyl)phenyl)thioureido)methyl)benzyl)phosphonium Acetate (NOTA-Bn-xy-TPP). TPP-xy-NH₂ (5.0 mg, 0.01 mmol) and p-Bn-SCN-NOTA (4.9 mg, 0.01 mmol) were dissolved in 2 mL of the 50% DMF/H₂O mixture. The pH was adjusted to 8.5 with 1 N NaOH. The mixture was stirred at room temperature overnight. After purification (method 2), the collected fractions at ~15.1 min were combined and lyophilized to give a white powder (4.9 mg, 50.9%). ¹H NMR (in D₂O): 2.42–3.82 (m, 19H), 4.42 (s, 2H, CH₂NH), 4.51 (d, 2H, PCH₂, J_{PH} = 13.8 Hz), 6.71 (m, 2H), 6.82–7.16 (m, 6H), 7.37–7.52 (m, 12H), 7.61 (m, 3H). ³¹P NMR: 25.80 (s). ESI-MS: *m/z* = 832.29 for [M]⁺ (calcd 832 for [C₄₆H₅₁N₅O₆PS]⁺). Anal. Calcd for C₄₆H₅₁N₅O₆PS·CH₃CO₂·H₂O: C, 63.35; H, 6.20; N, 7.70. Found: C, 63.28; H, 6.04; N, 7.86.

Cu(DO2A-xy-TPP)OAc. DO2A-xy-TPP (45.7 mg, 0.07 mmol) and Cu(OAc)₂·2H₂O (20.0 mg, 0.10 mmol) were dissolved in 5 mL of H₂O and 0.5 mL of 0.5 M NH₄OAc buffer (pH = 6.0). The solution was heated at 100 °C for 45 min. After cooling to room temperature, diethyl ether (25 mL) was added to the filtrate above slowly. The precipitate was separated and dried under vacuum overnight before being submitted for elemental analysis. The yield was 33.6 mg (67%). IR (cm⁻¹, KBr pellet): 1613 (s, ν_{C=O}), 1715 (s, ν_{C=O}), and 3412 (bs, ν_{O-H}). ESI-MS (positive mode): *m/z* = 715.30 for [M + H]⁺ (716 calcd for [C₃₈H₄₄CuN₄O₄P]⁺). Anal. Calcd for C₃₈H₄₃CuN₄O₄·CH₃CO₂·2H₂O: C, 59.69; H, 6.12; N, 7.24. Found: C, 59.97; H, 6.37; N, 7.00.

⁶⁴Cu-Labeling and Dose Preparation. To a 5 mL vial were added 50 μg of the TPP conjugate dissolved in 0.5 mL of 0.1 M NaOAc buffer (pH = 6.9) and 0.12 mL of ⁶⁴CuCl₂ solution (1.0–2.0 mCi) in 0.05 N HCl. The final pH in the reaction mixture was 5.0–5.5. The reaction mixture was then heated at 100 °C for 30 min. After cooling to room temperature, a sample of resulting solution was analyzed by radio-HPLC (method 2). The radiochemical purity (RCP) was >90% for all six ⁶⁴Cu radiotracers with the specific activity of ~50 Ci/mmol. All ⁶⁴Cu radiotracers were purified by HPLC before being used for biodistribution studies. The dose solution was prepared by dissolving the HPLC-purified radiotracer in saline to 10–25 μCi/mL. For the imaging study, ⁶⁴Cu(DO3A-bu-TPP) was first prepared and the resulting reaction mixture was used without purification. The mixture was diluted with saline to a concentration of ~5 mCi/mL.

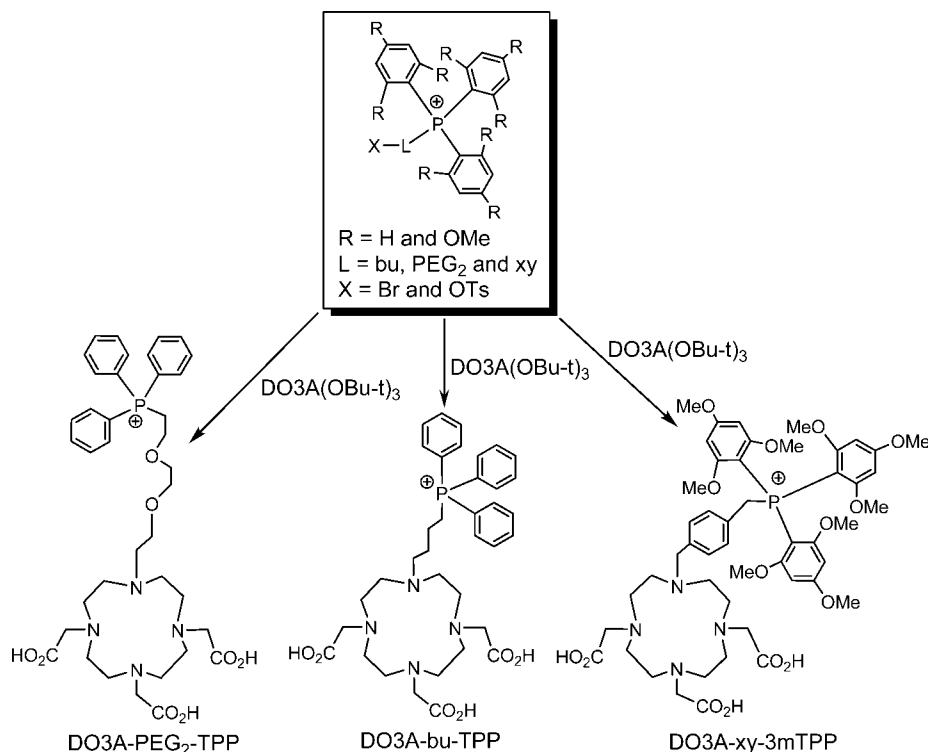
Solution Stability. The solution stability of ⁶⁴Cu(DO3A-bu-TPP), ⁶⁴Cu(DO2A-xy-TPP)⁺, and ⁶⁴Cu(NOTA-Bn-xy-TPP) were studied using the EDTA challenge experiment. The ⁶⁴Cu radiotracers were first prepared and then purified by HPLC. After removal of volatiles in the HPLC mobile phase, they were dissolved in 25 mM phosphate buffer (pH = 7.4) containing EDTA (1 mg/mL) to 1 mCi/mL. Samples of the resulting solution were analyzed by radio-HPLC at 0, 1, 2, 4, and 12 h post-purification.

Partition Coefficient. All ⁶⁴Cu radiotracers were purified by HPLC. HPLC purification is needed to eliminate potential interference from other radioimpurities. After complete removal of volatiles in the HPLC mobile phase, the residue was dissolved in a mixture of 3 mL of saline and 3 mL of *n*-octanol in a round-bottom flask. The mixture was vigorously stirred for 20 min at room temperature and was then transferred to a 15 mL Falcon conical tube. The tube was centrifuged at 12 500 rpm for 5 min. Samples in triplets from *n*-octanol and aqueous layers were obtained and were counted on a γ-counter (Perkin-Elmer Wizard 1480). The log *P* value was reported as an average of the data obtained in three independent measurements.

Animal Model and Biodistribution Protocol. Biodistribution studies were performed using athymic nude mice bearing U87MG human glioma xenografts in compliance with the NIH animal experiment guidelines (*Principles of Laboratory Animal Care*, NIH Publication No. 86-23, revised 1985). The animal protocol has been approved by Purdue University Animal Care and Use Committee (PACUC). Female athymic nu/nu mice were purchased from Harlan (Charles River, MA) at 4–5 weeks of age. The mice were orthotopically implanted with 5 × 10⁶ U87MG human glioma cells into the mammary fat pad. Four weeks after inoculation, the tumor size was in the range 0.3–0.8 g, and animals were used for biodistribution and imaging studies. Sixteen tumor-bearing mice (20–25 g) were randomly divided into four groups, each of which had four animals. The HPLC-purified ⁶⁴Cu radiotracer (~2.5 μCi dissolved in 0.1 mL of saline) was administered to each animal via tail vein. Four animals were euthanized by sodium pentobarbital overdose (100–200 mg/kg), exsanguinations, and opening of the thoracic cavity at 5, 30, 60, and 120 min postinjection (p.i.). Blood samples were withdrawn from the heart through a syringe. Organs were excised, washed with saline, dried with absorbent tissue, weighed, and counted on a γ-counter (Perkin-Elmer Wizard 1480). Organs of interest included tumor, brain, heart, spleen, lungs, liver, kidneys, muscle, and intestine. The organ uptake was calculated as a percentage of the injected dose per gram of organ tissue (% ID/g).

Calibration of microPET. Scanner activity calibration was performed to map between microPET image units and units of activity concentration. A preweighed 50 mL centrifuge tube was filled with a solution containing ⁶⁴CuCl₂ (~9.3 MBq as determined by the dose calibrator), which was used to simulate the whole body of the mouse. This tube was weighed, centered in the scanner aperture, and imaged for a 30 min static image. From the sample weight and assuming a density of 1 g/mL, the activity concentration in the bottle was calculated in units of μCi/mL. Eight planes were acquired in the coronal section. A rectangular region of interest (ROI) (counts/pixel/s) was drawn on the middle of 8 coronal planes. Using these data, a calibration factor was obtained by dividing the known radioactivity in the cylinder (μCi/mL) by the image ROI. This calibration factor was determined periodically and did not vary significantly with time.

MicroPET Imaging. MicroPET imaging of the tumor-bearing mice was performed using a microPET R4 rodent model scanner (Concorde Microsystems, Knoxville, TN). The U87MG tumor-bearing mice (*n* = 3) were imaged in the prone position in the microPET scanner. The tumor-bearing mice were injected with ~250 μCi of ⁶⁴Cu(DO3A-bu-TPP) via the tail vein, then anesthetized with 2% isoflurane and placed near the center of the FOV, where the highest resolution and sensitivity are obtained. Multiple static scans were obtained at 0.5, 1.0, 2, and 20 h p.i. The images were reconstructed by a two-dimensional ordered subsets expectation maximum (OSEM) algorithm. No correction was necessary for attenuation or scatter. At each microPET scan, the ROIs were drawn over the tumor and major organs on decay-corrected whole-body coronal images. The average radioactivity concentration within the tumor or an organ was obtained from mean pixel values within the multiple ROI volume, which were converted to counts/mL/min by using the calibration constant *C*. Assuming a tissue density of 1 g/mL, the ROIs were converted to counts/g/min and were then

Chart 1. Synthesis of DO3A-Conjugated TPP and TPA Cations

divided by the total administered activity to obtain an imaging ROI-derived percentage administered activity per gram of tissue (% ID/g).

Metabolism. The metabolic stability of ⁶⁴Cu(DO2A-xy-TPP)⁺, ⁶⁴Cu(DO3A-PEG₂-TPP), and ⁶⁴Cu(NOTA-Bn-xy-TPP) was evaluated in normal athymic nude mice. Two animals were used for each radiotracer. Each mouse was administered with the ⁶⁴Cu radiotracer at a dose of 100 μCi in 0.2 mL of saline via tail vein. The urine samples were collected at 30 and 120 min p.i. by manual void and were mixed with equal volume of acetonitrile. The mixture was centrifuged at 8000 rpm. The supernatant was collected and filtered through a 0.20 μm Millex-LG syringe-driven filter unit to remove the precipitate and large proteins. The filtrate was analyzed by radio-HPLC (method 2). The feces samples were collected at 120 min p.i. and were suspended in the 50% acetonitrile aqueous solution. The mixture was vortexed for 5–10 min. After centrifuging at 8000 rpm for 5 min, the supernatant was collected and passed through a 0.20 μm Millex-LG syringe-driven filter unit to remove the precipitate or particles. The filtrate was then analyzed by radio-HPLC (method 2).

Stability of ⁶⁴Cu(DO3A-PEG₂-TPP) in Liver. The liver tissue was harvested at 120 min p.i. from the mouse administered with ⁶⁴Cu(DO3A-PEG₂-TPP) (~100 μCi), counted in a γ-counter for the total liver radioactivity, cut into small pieces, and then homogenized. The homogenate was mixed with 2 mL of saline. After centrifuging at 8000 rpm for 5 min, the supernatant was collected and counted with a γ-counter to determine the radioactivity recovery. After filtration through a 0.20 μm Millex-LG syringe-driven filter unit to remove the precipitate or particles, the filtrate was then analyzed by radio-HPLC (method 2).

Data and Statistical Analysis. The biodistribution data and target-to-background (T/B) ratios are reported as an average plus the standard variation based on results from four tumor-bearing mice at each time point. Comparison between two different radiotracers was made using the two-way ANOVA test (GraphPad Prim 5.0, San Diego, CA). The level of significance was set at $p < 0.05$.

Results

Synthesis of TPP Conjugates. Synthesis of TPP conjugates was straightforward. DO3A-bu-TPP, DO3A-xy-3mTPP, and

DO3A-PEG₂-TPP were prepared according to Chart 1. They were designed to examine the linker effects on organ uptake and excretion kinetics of their ⁶⁴Cu complexes. DO2A-xy-TPP and DO2A-(xy-TPP)₂ were isolated from the same reaction (Chart 2) between DO2A(t-Bu)₂ and TPP-xy-Br in 1:1 molar ratio in the presence of triethylamine. DO2A-xy-TPP was designed to explore the impact of molecular charge of ⁶⁴Cu chelates (⁶⁴Cu-DO3A versus ⁶⁴Cu-DO2A) on biological properties of ⁶⁴Cu radiotracers. DO2A-(xy-TPP)₂ was designed to test if the extra TPP moiety will result in any added benefits with respect to the tumor uptake and T/B ratios. NOTA-Bn-xy-TPP was prepared according to Chart 3 by reacting p-SCN-Bn-NOTA with TPP-xy-NH₂ in a mixture of DMF/water (50:50 = v/v) under slightly basic conditions (pH = 8.5). It was designed to examine the impact of BFCs (DO3A versus NOTA-Bn) on biodistribution characteristics of the ⁶⁴Cu radiotracer. All six newly synthesized TPP conjugates were purified by HPLC (method 1) and had an HPLC purity of >95% before being used for ⁶⁴Cu-labeling. After lyophilization, they were all obtained as their acetate salts since the HPLC mobile phases contain 1% acetic acid. They all have been characterized by NMR (¹H, ¹³C, and ³¹P), ESI-MS, and elemental analysis (C, H, and N).

Synthesis and Characterization of Cu(DO2A-xy-TPP)(OAc). Cu(DO2A-xy-TPP)⁺ is used as a model compound for structural characterization of ⁶⁴Cu(DO2A-xy-TPP)⁺. It was prepared by reacting DO2A-xy-TPP with 1 equiv of Cu(II) acetate in 0.5 M ammonium acetate buffer (pH = 6), was isolated as its acetate salt, and has been characterized by IR, ESI-MS, and elemental analysis. The IR spectrum of Cu(DO2A-xy-TPP)(OAc) shows a broad band at 3432 cm⁻¹ due to the crystallization water, a strong band at 1721 cm⁻¹ due to the acetate counterion, and a strong band at 1637 cm⁻¹ from two coordinated carboxylate groups. The ESI-MS spectrum of Cu(DO2A-xy-TPP)⁺ displays a molecular ion at $m/z = 715.30$ for [M + H]⁺. Attempts to grow crystals for structural

Chart 2

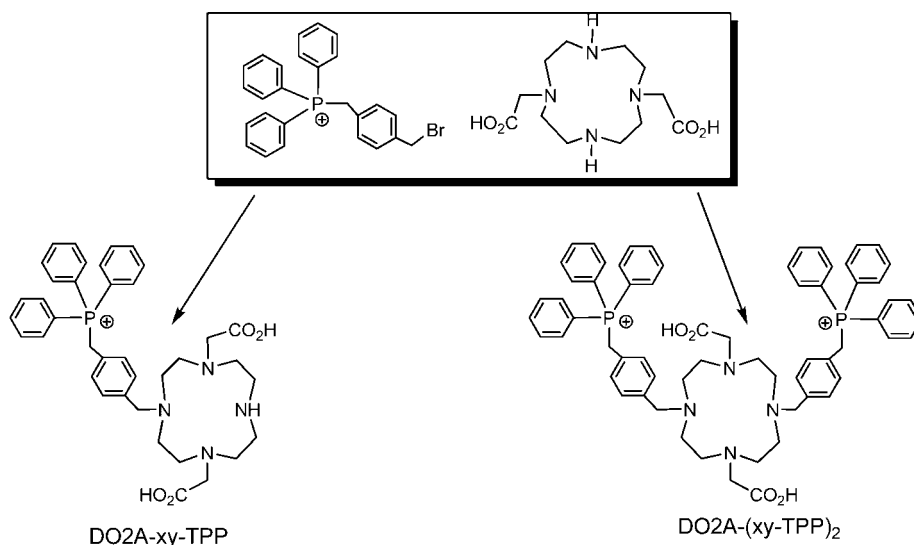
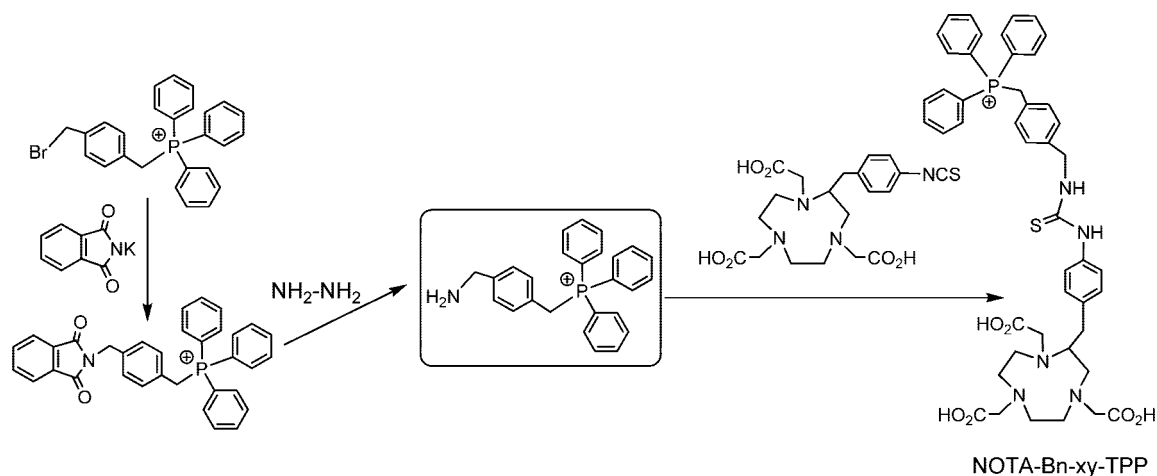


Chart 3



determination of Cu(DO2A-xy-TPP)(OAc) by X-ray crystallography were unsuccessful. Unlike DO3A, which forms anionic Cu-DO3A chelate,⁴⁴ DO2A-xy-TPP has only two acetate chelating arms. Coordination of these two carboxylate-O atoms will result in formation of a neutral Cu-DO2A chelate. Thus, Cu(DO2A-xy-TPP)⁺ is cationic with a positive charge on TPP. On the basis of elemental analysis and IR spectroscopic data, we believe that Cu(DO2A-xy-TPP)⁺ exists as its acetate salt form in the solid state.

Radiochemistry. All ⁶⁴Cu radiotracers were prepared by reacting ⁶⁴CuCl₂ with the TPP conjugate in 0.1 M NaOAc buffer (pH = 6.9) at 100 °C for 30 min and were analyzed using the same reversed-phase HPLC method (method 2). The RCP was >90%, with the specific activity being >50 Ci/mmol for all new ⁶⁴Cu radiotracers. Their partition coefficients were determined in a 50%:50% (v/v) mixture of *n*-octanol and 25 mM phosphate buffer (pH = 7.4). Their calculated log *P* values and HPLC retention times are listed in Table 1. As the number of methoxy groups increases, the lipophilicity of ⁶⁴Cu radiotracer was significantly increased from ⁶⁴Cu(DO3A-xy-TPP) (log *P* = -2.67 ± 0.21)³⁹ to ⁶⁴Cu(DO3A-xy-mTPP) (log *P* = -2.02 ± 0.05),³⁹ and ⁶⁴Cu(DO3A-xy-3mTPP) (log *P* = -1.89 ± 0.02). Replacing xylene (xy) with a butylene (bu) linker resulted in a reduction of lipophilicity for the ⁶⁴Cu radiotracer: ⁶⁴Cu(DO3A-bu-TPP) (log *P* = -2.98 ± 0.36). Substitution of xylene with

Table 1. HPLC Retention Time and log *P* Values for the ⁶⁴Cu-Labeled TPP Cations

compound	RCP (%)	retention time (min)	log <i>P</i> value
⁶⁴ Cu(DO3A-xy-TPP)	>95	15.6	-2.67 ± 0.21
⁶⁴ Cu(DO3A-xy-mTPP)	>98	20.9	-2.02 ± 0.01
⁶⁴ Cu(DO3A-bu-TPP)	>95	15.5	-2.98 ± 0.36
⁶⁴ Cu(DO3A-PEG ₂ -TPP)	>96	18.2	-2.81 ± 0.07
⁶⁴ Cu(DO3A-xy-3mTPP)	>97	17.5	-1.89 ± 0.02
⁶⁴ Cu(DO2A-xy-TPP) ⁺	>97	18.2	-2.51 ± 0.18
⁶⁴ Cu(DO2A-(xy-TPP) ₂) ²⁺	>95	22.0	-1.23 ± 0.01
⁶⁴ Cu(NOTA-Bn-xy-TPP)	>98	17.4	-1.90 ± 0.15

the PEG₂ linker did not change the lipophilicity of ⁶⁴Cu(DO3A-PEG₂-TPP) (log *P* = -2.81 ± 0.07) vs ⁶⁴Cu(DO3A-xy-TPP) (log *P* = -2.67 ± 0.21). ⁶⁴Cu(NOTA-Bn-xy-TPP) (log *P* = -1.90 ± 0.15) is more lipophilic than ⁶⁴Cu(DO3A-xy-TPP), due to the presence of an extra aromatic benzoyl group. Since NOTA-Bn-xy-TPP has the same number of acetate chelating arms as DO3A-xy-TPP, it is expected to form the ⁶⁴Cu chelate, in which ⁶⁴Cu is coordinated either by N₃O₃ donor atoms in the distorted octahedral coordination geometry or by N₃O₂ donor atoms in the square-pyramidal coordination sphere with one carboxylate-O atom being uncoordinated and deprotonated. It is reasonable to believe that ⁶⁴Cu(NOTA-Bn-xy-TPP) exists in solution as its Zwitterion form.

Table 2. Solution Stability Data for the HPLC-Purified ⁶⁴Cu-Labeled TPP Cations in the Presence of Excess EDTA (1 mg/mL in 25 mM phosphate buffer, pH = 7.5)

	time post-purification				
	0.5 h	1 h	2 h	4 h	12 h
⁶⁴ Cu(DO3A-xy-TPP)	99	99	98	98	97
⁶⁴ Cu(DO2A-xy-TPP) ⁺	99	98	98	97	95
⁶⁴ Cu(NOTA-Bn-xy-TPP)	98	98	99	98	97

Solution Stability. The EDTA challenge experiment was used to study solution stability of ⁶⁴Cu(DO2A-xy-TPP)⁺, ⁶⁴Cu(DO3A-PEG₂-TPP), and ⁶⁴Cu(NOTA-Bn-xy-TPP). These three ⁶⁴Cu radiotracers were selected because they represent three different types of BFCs for ⁶⁴Cu chelation. The purpose of these studies was to demonstrate that the ⁶⁴Cu radiotracer remains intact before being injected into the tumor-bearing mice. Table 2 summarizes the solution stability data for the HPLC-purified ⁶⁴Cu(DO2A-xy-TPP)⁺, ⁶⁴Cu(DO3A-PEG₂-TPP), and ⁶⁴Cu(NOTA-Bn-xy-TPP) in the presence of excess EDTA (3 mM, pH = 7.4). It is quite clear that all three ⁶⁴Cu radiotracers remain stable for >12 h in the presence of excess EDTA, which is completely consistent with their metabolic stability during excretion from normal mice.

Biodistribution Data. Biodistribution characteristics of all six new ⁶⁴Cu radiotracers were evaluated in the athymic nude mice bearing subcutaneous U87MG human glioma xenografts. Detailed biodistribution data and T/B ratios for these six ⁶⁴Cu radiotracers are listed in Tables SI–SVI. The organ uptake is expressed as an average % ID/g plus the standard variation based on results from four tumor-bearing mice (n = 4) at each time point. The main objective of these studies was to explore the impact of TPP moieties, linkers, bifunctional chelators, and overall molecular charge on biodistribution characteristics and excretion kinetics of the ⁶⁴Cu-labeled TPP cations.

Comparison with ^{99m}Tc-Sestamibi. Figures 2 and 3 compare the organ uptake and T/B ratios between the ⁶⁴Cu radiotracers and ^{99m}Tc-sestamibi in the tumor, heart, liver, and muscle. The biodistribution data and T/B ratios for ^{99m}Tc-sestamibi were obtained from our previous report.³⁹ ^{99m}Tc-Sestamibi has been clinically used for tumor imaging and for monitoring the MDR transport function in tumors of different origin.^{17–29} This comparison allows us to demonstrate that the ⁶⁴Cu-labeled TPP cations described in this study have significant advantages over ^{99m}Tc-sestamibi with respect to their organ uptake and T/B ratios.

The most striking differences between ⁶⁴Cu-labeled TPP cations and ^{99m}Tc-sestamibi are their uptake in the heart and muscle (Figure 2) and their tumor/heart, tumor/lung, and tumor/muscle ratios (Figure 3). For example, the heart uptake was <1% ID/g for all six ⁶⁴Cu radiotracers at >30 min p.i., while the heart uptake of ^{99m}Tc-sestamibi was 19.22 ± 7.62 at 5 min p.i. and 19.19 ± 5.32% ID/g at 120 min p.i.³⁹ The tumor/heart ratios of ⁶⁴Cu(DO3A-bu-TPP), ⁶⁴Cu(DO3A-PEG₂-TPP), and ⁶⁴Cu(DO2A-xy-TPP)⁺ were steadily increased from ~1 at 5 min p.i. to ~4 at 120 min p.i. ⁶⁴Cu(DO2A-xy-TPP)⁺ and ^{99m}Tc-sestamibi had very similar tumor uptake over the 2 h period (Figure 2), but the tumor/heart ratio of ⁶⁴Cu(DO2A-xy-TPP)⁺ at 120 min p.i. was about 40-fold better than that of ^{99m}Tc-sestamibi. The tumor/heart ratios of ⁶⁴Cu(NOA-Bn-xy-TPP) and ⁶⁴Cu(DO3A-(xy-TPP)₂)²⁺ were very low due to their low tumor uptake. ⁶⁴Cu(DO3A-xy-3mTPP) had the best tumor/heart ratio at >60 min p.i. The muscle uptake of the ⁶⁴Cu-labeled TPP cations was almost undetectable at >30 min p.i. In contrast, ^{99m}Tc-sestamibi has a high muscle uptake (4.84 ± 1.22 and 5.45 ± 1.24% ID/g at 5 and 120 min p.i., respectively). The lung uptake of the ⁶⁴Cu radiotracers was also significantly lower (p < 0.01) than that of ^{99m}Tc-sestamibi at 5–60 min p.i. (Tables SI–VI), and their tumor/lung ratios were better than those of

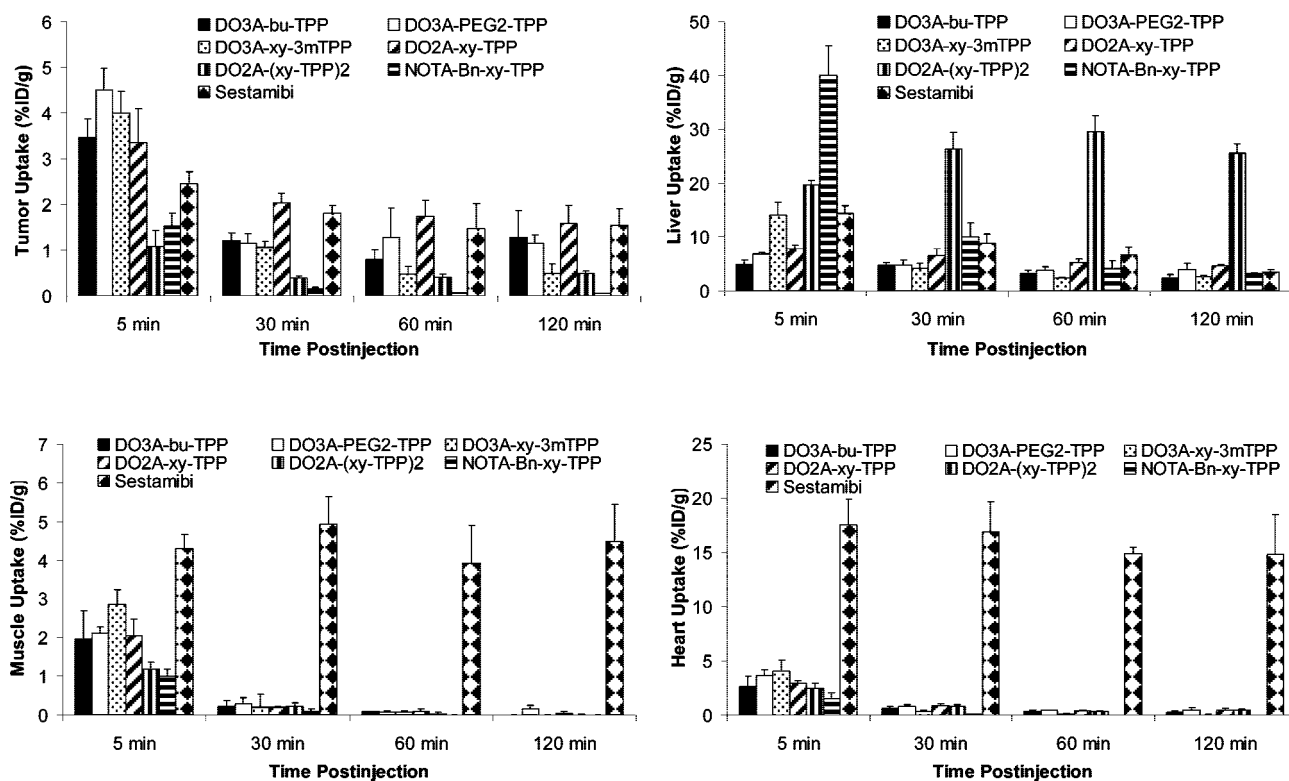


Figure 2. Direct comparison of organ (tumor, heart, liver, and muscle) uptake between the ⁶⁴Cu-labeled TPP cations and ^{99m}Tc-sestamibi in athymic nude mice (n = 4) bearing U87MG human glioma xenografts. The most striking difference between the ⁶⁴Cu-labeled TPP cations and ^{99m}Tc-sestamibi is their uptake in the heart and muscle.

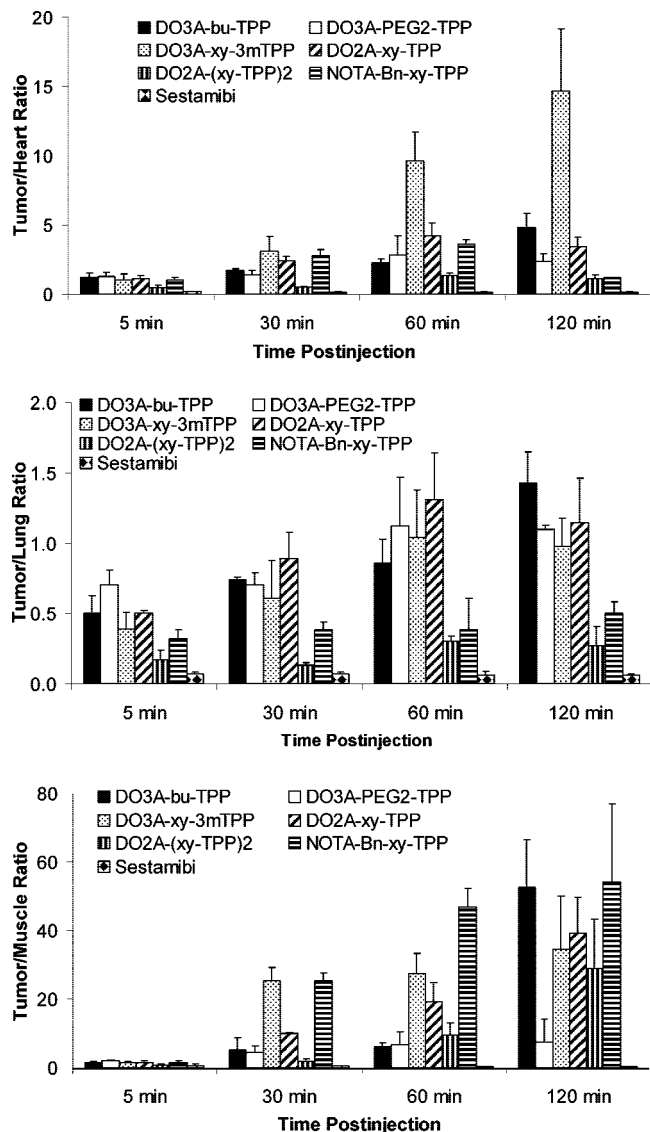


Figure 3. Direct comparison of tumor-to-background ratios between the ^{64}Cu -labeled TPP cations and $^{99\text{m}}\text{Tc}$ -sestamibi in athymic nude mice bearing U87MG human glioma xenografts. The most significant difference between the ^{64}Cu -labeled TPP cations and $^{99\text{m}}\text{Tc}$ -sestamibi is their tumor/heart, tumor/lung, and tumor/muscle ratios.

$^{99\text{m}}\text{Tc}$ -sestamibi (Figure 3) over the 2 h study period. Among the six new ^{64}Cu radiotracers, $^{64}\text{Cu}(\text{DO2A-xy-TPP})^+$ is probably the best considering its uptake in the tumor and liver.

Impact of TPP Cations. Figure 4 shows the impact of TPP cations on the radiotracer tumor uptake and T/B ratios. Biodistribution data and T/B ratios for $^{64}\text{Cu}(\text{DO3A-xy-TPP})$ and $^{64}\text{Cu}(\text{DO3A-xy-mTPP})$ were obtained from our previous report.³⁹ $^{64}\text{Cu}(\text{DO3A-xy-mTPP})$ has the liver uptake significantly lower ($p < 0.01$) than that of $^{64}\text{Cu}(\text{DO3A-xy-TPP})$. Even though the tumor uptake of $^{64}\text{Cu}(\text{DO3A-xy-3mTPP})$ is the lowest, its tumor/heart ratio is the best at >60 min p.i. The addition of extra methoxy groups on the TPP improves the radiotracer clearance from the liver and lungs, but it also resulted in a significant washout from the tumor. As a result, the tumor/lung ratios of $^{64}\text{Cu}(\text{DO3A-xy-TPP})$, $^{64}\text{Cu}(\text{DO3A-xy-mTPP})$, and $^{64}\text{Cu}(\text{DO3A-xy-3mTPP})$ were well within the experimental error (Figure 4). It seems that mTPP is better than TPP and 3mTPP as the mitochondrion-targeting molecules considering both the tumor uptake and tumor/liver ratios of their corresponding ^{64}Cu radiotracers.

Impact of ^{64}Cu Chelate. Because of its d^9 electron configuration, $\text{Cu}(\text{II})$ complexes are often kinetically labile with respect to dissociation. The BFCs for copper radionuclides have been focused on macrocyclic chelators that form $\text{Cu}(\text{II})$ complexes with very high thermodynamic stability and kinetic inertness.^{45–50} Since the ^{64}Cu chelate is a major part of the ^{64}Cu radiotracer, we performed biodistribution studies on $^{64}\text{Cu}(\text{DO2A-xy-TPP})^+$, $^{64}\text{Cu}(\text{DO2A-(xy-TPP)}_2)^{2+}$, and $^{64}\text{Cu}(\text{NOTA-Bn-xy-TPP})$ in athymic nude mice bearing U87MG human glioma xenografts. Figure 5 shows the impact of the ^{64}Cu chelate on both tumor uptake and T/B ratios of ^{64}Cu radiotracers. Biodistribution data and T/B ratios of $^{64}\text{Cu}(\text{DO3A-xy-TPP})$ were obtained from our previous report.³⁹ $^{64}\text{Cu}(\text{DO3A-xy-TPP})$ and $^{64}\text{Cu}(\text{DO2A-xy-TPP})^+$ have very similar lipophilicity ($\log P = -2.67 \pm 0.21$ and -2.51 ± 0.18 , respectively) in spite of their difference in molecular charge. Their tumor uptake and tumor/heart and tumor/lung ratios compared well over the 2 h period. However, the liver uptake of $^{64}\text{Cu}(\text{DO2A-xy-TPP})^+$ was significantly lower ($p < 0.01$) and its tumor/liver ratios were much better than that $^{64}\text{Cu}(\text{DO3A-xy-TPP})$ at all four time points. Because of the extra xy-TPP moiety, $^{64}\text{Cu}(\text{DO2A-(xy-TPP)}_2)^{2+}$ is most likely dicationic, and its lipophilicity ($\log P = -1.23 \pm 0.01$) is higher than that of $^{64}\text{Cu}(\text{DO2A-xy-TPP})^+$ ($\log P = -2.51 \pm 0.18$). As a result, $^{64}\text{Cu}(\text{DO3A-(xy-TPP)}_2)^{2+}$ has a much higher liver uptake and lower tumor uptake than $^{64}\text{Cu}(\text{DO2A-xy-TPP})^+$ and $^{64}\text{Cu}(\text{DO3A-xy-TPP})$. $^{64}\text{Cu}(\text{NOTA-Bn-xy-TPP})$ has the same overall molecular charge as $^{64}\text{Cu}(\text{DO3A-xy-TPP})$, but its tumor uptake and tumor/heart ratios were significantly lower ($p < 0.01$) than those of $^{64}\text{Cu}(\text{DO3A-xy-TPP})$ at all four time points. These data clearly demonstrated that the ^{64}Cu chelates have a significant impact on the radiotracer tumor uptake and T/B ratios.

Linker Effects. Figure 6 illustrates the linker effects on tumor uptake and tumor/heart ratios of ^{64}Cu radiotracers. The tumor uptake of $^{64}\text{Cu}(\text{DO3A-bu-TPP})$ ($1.29 \pm 0.58\%$ ID/g) was significantly lower ($p < 0.01$) than that of $^{64}\text{Cu}(\text{DO3A-xy-TPP})$ ($2.51 \pm 0.38\%$ ID/g) at 120 min p.i., but their tumor/heart ratios were almost identical (4.80 ± 1.04 and 4.25 ± 0.23 , respectively). Substitution of xylene with the PEG_2 linker also led to a significant reduction of the radiotracer in the liver and higher tumor/liver ratios, even though $^{64}\text{Cu}(\text{DO3A-PEG}_2\text{-TPP})$ and $^{64}\text{Cu}(\text{DO3A-xy-TPP})$ have similar lipophilicity (Table 1).

PET Imaging. We performed a microPET imaging study on $^{64}\text{Cu}(\text{DO3A-bu-TPP})$ using athymic nude mice ($n = 3$) bearing U87MG human glioma xenografts. Figure 7 illustrates the coronal microPET images (A) and the activity accumulation quantification (B) in several organs of the tumor-bearing mice administered with ~ 250 mCi of $^{64}\text{Cu}(\text{DO3A-bu-TPP})$. The tumor was clearly visualized as early as 30 min p.i. with very high tumor-to-background contrast. No significant radioactivity accumulation was detected in the brain. The radioactivity accumulation in the heart and muscle was also very low. After normalization, the tumor uptake of $^{64}\text{Cu}(\text{DO3A-bu-TPP})$ is $1.29 \pm 0.57\%$, $1.22 \pm 0.73\%$, $1.31 \pm 0.55\%$, and $1.14 \pm 0.56\%$ ID/g at 3 min, 1.4 h, 3.9 h, and 20.5 h p.i., respectively. These data are completely consistent with those obtained in the ex vivo biodistribution study (Table SI).

Metabolic Properties. Metabolism studies were performed using normal athymic nude mice on $^{64}\text{Cu}(\text{DO2A-xy-TPP})^+$, $^{64}\text{Cu}(\text{DO3A-PEG}_2\text{-TPP})$, and $^{64}\text{Cu}(\text{NOTA-Bn-xy-TPP})$. These three ^{64}Cu radiotracers were selected because of BFCs for ^{64}Cu chelation. Each mouse was administered with ~ 100 μCi of the ^{64}Cu radiotracer. Since they were excreted from renal and hepatobiliary routes, we collected both urine and feces samples

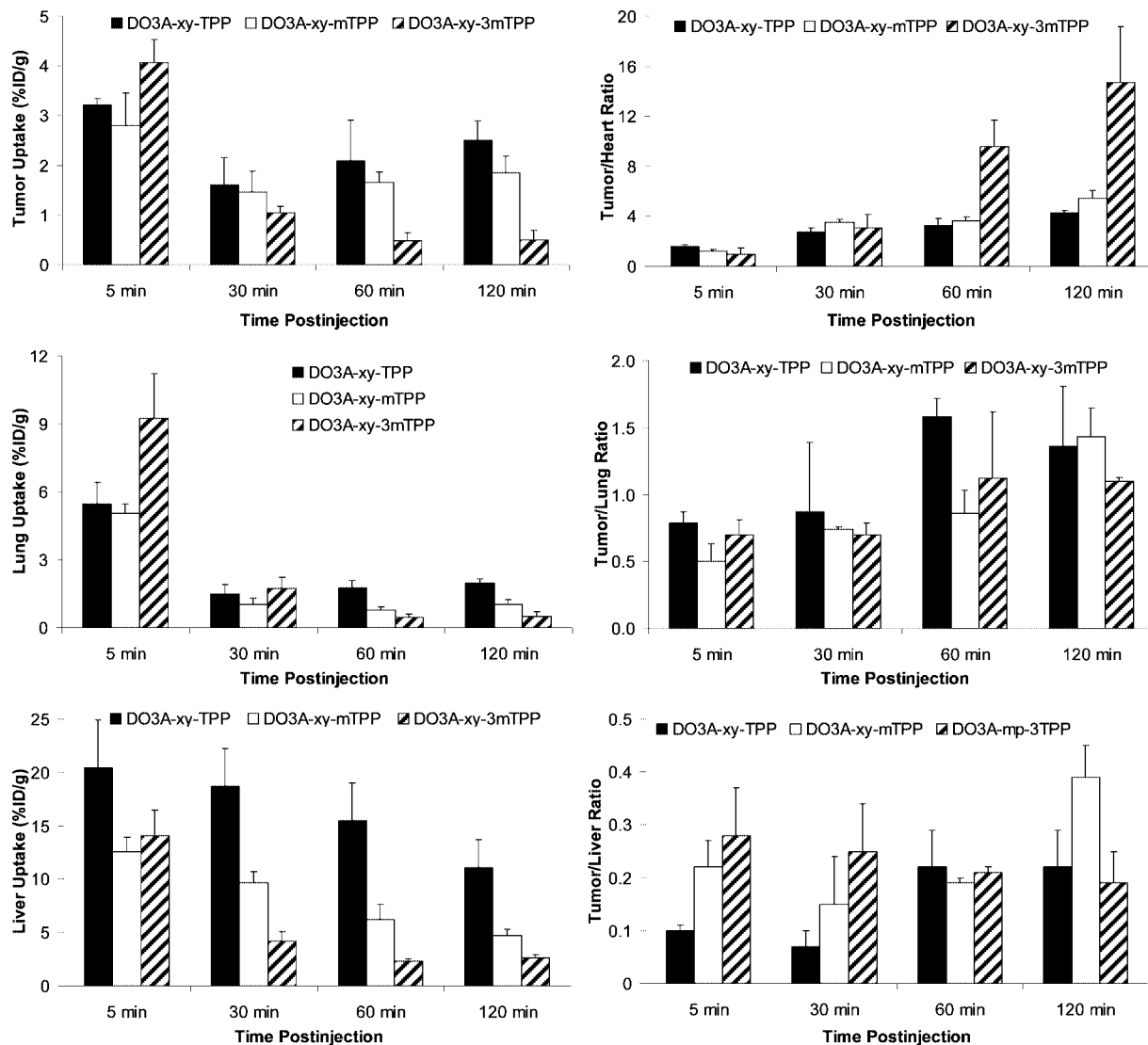


Figure 4. Impact of TPP moieties on tumor uptake and tumor/heart ratios of the ⁶⁴Cu-labeled TPP cations in nude mice bearing U87MG human glioma xenografts (n = 4).

and analyzed them by a reversed-phase HPLC method to determine if they are able to retain their chemical integrity. Figure 8 illustrates radio-HPLC chromatograms of ⁶⁴Cu(DO3A-PEG₂-TPP) (left) and ⁶⁴Cu(DO3A-Bn-xy-TPP) (right) in saline before injection (A), in the urine at 30 min p.i. (B), in the urine at 120 min p.i. (C), and in the feces at 120 min p.i. (D). There is no significant metabolite detectable in both urine and feces samples from the mice administered with either ⁶⁴Cu(DO3A-PEG₂-TPP) or ⁶⁴Cu(NOTA-Bn-xy-TPP). Similar metabolic stability was also observed for ⁶⁴Cu(DO2A-xy-TPP)⁺ (Figure SI).

Transchelation of ⁶⁴Cu(DO3A-PEG₂-TPP) in the Liver. We also examined the stability of ⁶⁴Cu(DO3A-PEG₂-TPP) in the liver. About 50% of total liver radioactivity was recovered in the homogenate. The supernatant was analyzed using the reversed-phase HPLC method (method 2). Figure SII shows the radio-HPLC chromatogram of the liver homogenate. There are two radiometric peaks at 5 and 10 min with no intact ⁶⁴Cu(DO3A-PEG₂-TPP), suggesting that it underwent extensive transchelation in the liver during the 2 h study period.

Discussion

In this study, we evaluated six new ⁶⁴Cu-labeled TPP cations using athymic nude mice bearing U87MG glioma xenografts

for their biodistribution characteristics and excretion kinetics and found that ⁶⁴Cu(DO3A-bu-TPP), ⁶⁴Cu(DO2A-xy-TPP)⁺, and ⁶⁴Cu(DO3A-PEG₂-TPP) have a tumor uptake comparable to that of ^{99m}Tc-sestamibi (Figure 2), but their T/B ratios are much better than those of ^{99m}Tc-sestamibi at all four time points (Figure 3). For example, the tumor/heart ratio of ⁶⁴Cu(DO2A-xy-TPP)⁺ is 1.13 ± 0.21 at 5 min p.i. and increases to 3.39 ± 0.23 at 120 min p.i., while the tumor/heart ratio of ^{99m}Tc-sestamibi is <0.2 during the 2 h period. The tumor/heart, tumor/lung, and tumor/muscle ratios of ⁶⁴Cu(DO2A-xy-TPP)⁺ are 25, 20, and 160 times, respectively, better than those ^{99m}Tc-sestamibi at 120 min p.i. The tumor/heart and tumor/liver ratios of ⁶⁴Cu(DO3A-bu-TPP) are more than 37- and 235-fold higher than those ^{99m}Tc-sestamibi.

While the enhanced mitochondrial potential provides the electrochemical driving force for cationic radiotracers to localize in the energized mitochondria of tumor cells, its lipophilicity is one of the main factors that control the diffusion kinetics for radiotracers to cross both plasma and mitochondrial membranes. For more lipophilic radiotracers, such as ^{99m}Tc-sestamibi (log P = 1.09 ± 0.15), their membrane diffusion kinetics are fast and they can localize quickly in the tumor and mitochondrion-rich organs, such as the heart, liver, and kidneys, and their tumor

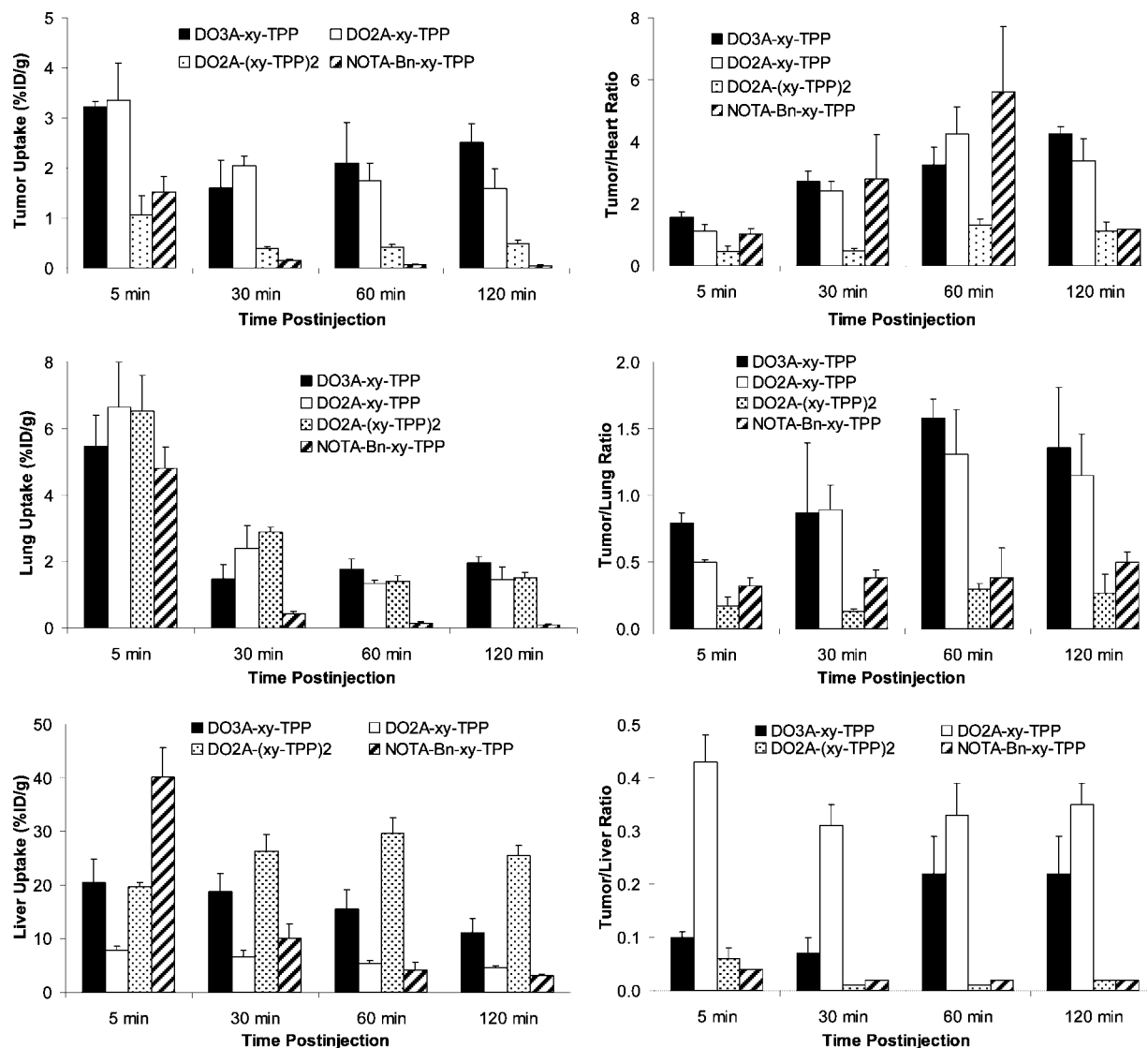


Figure 5. Impact of BFCs and their ^{64}Cu chelates on tumor uptake and tumor/heart ratios of the ^{64}Cu -labeled TPP cations in nude mice ($n = 4$) bearing U87MG human glioma xenografts.

selectivity is low. In contrast, the ^{64}Cu -labeled TPP cations, such as $^{64}\text{Cu}(\text{DO2A-xy-TPP})^+$ ($\log P = -2.51 \pm 0.18$), have very low lipophilicity and slow membrane penetration kinetics, as demonstrated in the *in vitro* assays using glioma cells and the isolated mitochondria from glioma cells.³⁹ As a result, most of the ^{64}Cu -labeled TPP cations tend to localize in the tumor, where the mitochondrial potential is elevated as compared to normal tissues such as the heart and muscle. It is not surprising that the ^{64}Cu radiotracers with $\log P$ values < -1.5 all have low uptake in the heart and muscle with very high tumor/heart and tumor/muscle selectivity.

In addition to lipophilicity, there are many other factors contributing to the differences in biological properties of ^{64}Cu radiotracers. The ^{64}Cu radiotracer described in this study contains a TPP cation, a linker, and a ^{64}Cu chelate ($^{64}\text{Cu} + \text{BFC}$), all of which affect its biodistribution and excretion kinetics from noncancerous organs. For example, introduction of methoxy groups on the TPP cation improves the radiotracer clearance from liver and lungs (Figure 4), but it also results in a significant washout from the tumor. Considering both tumor uptake and T/B ratios of ^{64}Cu radiotracers, mTPP is better than TPP and 3mTPP as the mitochondrion-targeting molecule. Replacing xylene with the butylene linker results in a significant reduction of the tumor uptake, but the tumor/heart and tumor/

lung ratios of the ^{64}Cu radiotracer remained relatively unchanged (Figure 6). More importantly, the use of a butylene linker results in a significant improvement of the tumor/liver ratio at 120 min (Figure 6) even though $^{64}\text{Cu}(\text{DO3A-bu-TPP})$ has a lower tumor uptake than $^{64}\text{Cu}(\text{DO3A-xy-TPP})$ at > 30 min p.i. This is further confirmed by the PET imaging study (Figure 7). $^{64}\text{Cu}(\text{DO3A-xy-TPP})$ and $^{64}\text{Cu}(\text{DO2A-xy-TPP})^+$ have very similar lipophilicity ($\log P = -2.67 \pm 0.21$ versus -2.51 ± 0.18) despite their charge difference. Their tumor uptake and tumor/heart and tumor/lung ratios compared well over the 2 h study period. However, the positive charge of $^{64}\text{Cu}(\text{DO2A-xy-TPP})^+$ results in a dramatic reduction in liver uptake, which leads to much better tumor/liver ratios than those of $^{64}\text{Cu}(\text{DO3A-xy-TPP})$ (Figure 5). It seems that an overall neutral molecular charge is not required to achieve high tumor uptake and high T/B ratios.

Addition of an extra TPP moiety makes $^{64}\text{Cu}(\text{DO3A-(xy-TPP)}_2)^{2+}$ more lipophilic than $^{64}\text{Cu}(\text{DO2A-xy-TPP})^+$. While the dicationic character might explain the low tumor uptake of $^{64}\text{Cu}(\text{DO3A-(xy-TPP)}_2)^{2+}$ (Figure 5), its high liver uptake is probably related to its high lipophilicity. From this point of view, monoanionic BFCs should be avoided to ensure that the ^{64}Cu chelate has a neutral or negative charge in order to maintain the high radiotracer tumor uptake.

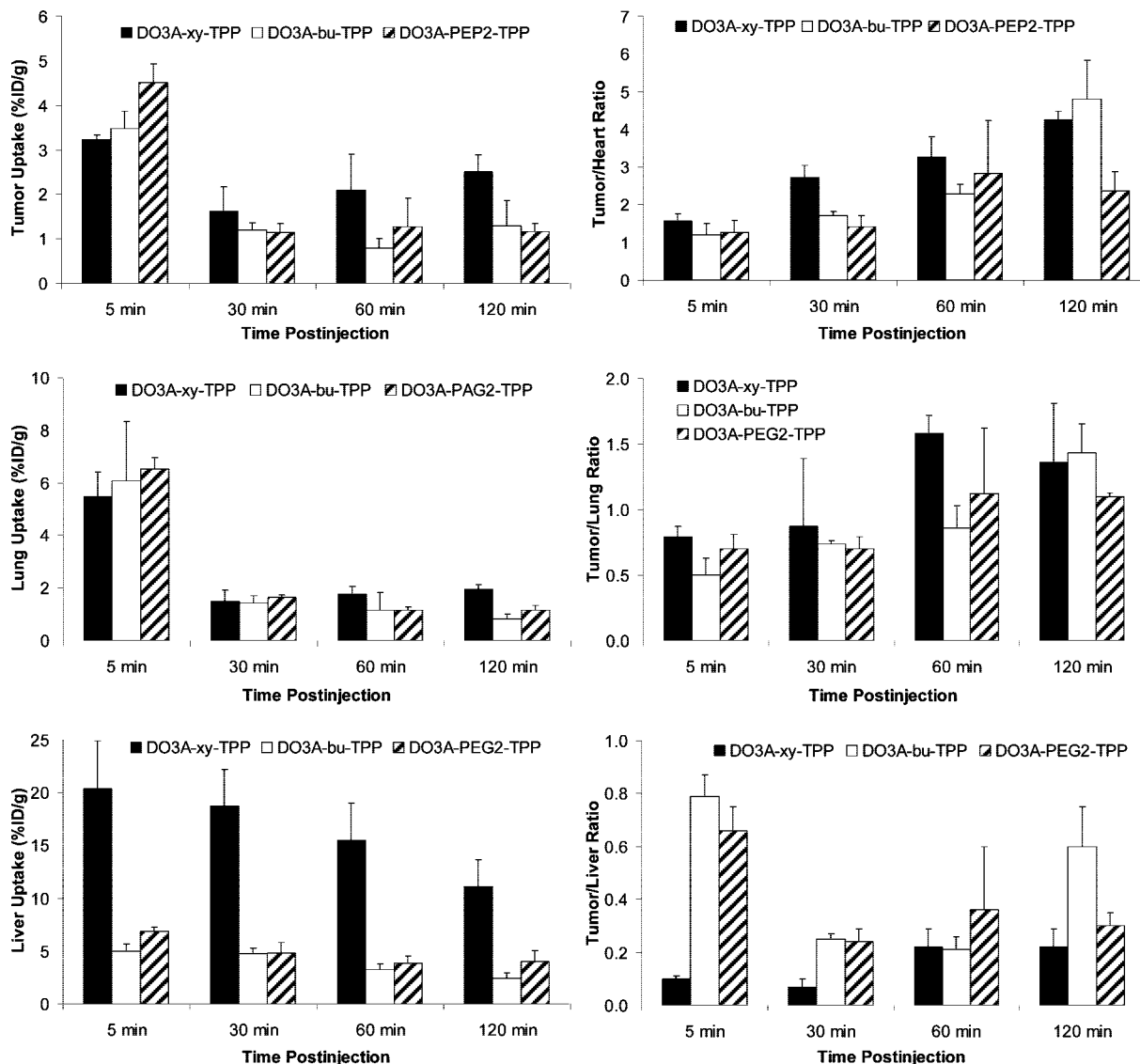


Figure 6. Impact of linkers on tumor uptake and tumor/heart ratios of ⁶⁴Cu radiotracers in nude mice bearing U87MG human glioma xenografts (*n* = 4).

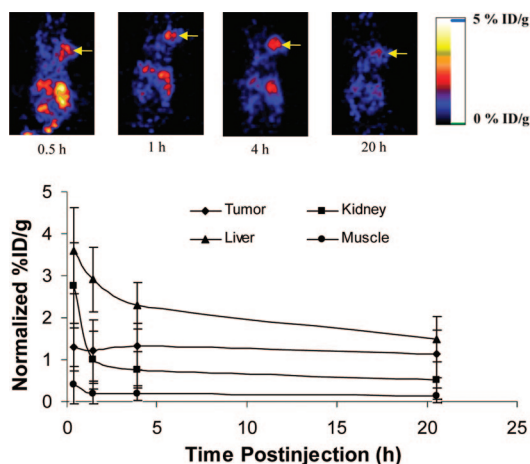


Figure 7. Decay-corrected whole-body coronal microPET images (top) and the radioactivity accumulation quantification (*n* = 3, mean ± SD) in selected organs (bottom) of athymic nude mice bearing U87MG tumor administered with ~250 μCi of ⁶⁴Cu(DO3A-bu-TPP). Arrows indicate the presence of glioma tumors.

Among all the ⁶⁴Cu radiotracers evaluated in this animal model, ⁶⁴Cu(NOTA-Bn-xy-TPP) has the lowest tumor uptake

at >30 min p.i. Since ⁶⁴Cu(NOTA-Bn-xy-TPP) ($\log P = -1.81 \pm 0.02$) has the same lipophilicity as ⁶⁴Cu(DO3A-xy-3mTPP) ($\log P = -1.90 \pm 0.15$), it is reasonable to believe that its low tumor uptake is probably caused by the ⁶⁴Cu-NOTA-Bn chelate. More detailed studies are needed to clarify the impact of the coordination chemistry in the ⁶⁴Cu chelate on tumor uptake and T/B ratios of the ⁶⁴Cu-labeled TPP cations.

Significant metabolic degradation has been detected in the feces of athymic nude mice administered with ⁶⁴Cu(DO3A-xy-TPP), and the metabolic instability is probably caused by cleavage of the TPP moiety.³⁹ For ⁶⁴Cu(DO3A-PEG₂-TPP) and ⁶⁴Cu(NOTA-Bn-xy-TPP), however, there was very little metabolism (<5%) detected in urine and feces samples (Figure 8), suggesting that the linker and BFC have a significant impact on the metabolic stability of ⁶⁴Cu radiotracers and that the ⁶⁴Cu radiotracer is able to maintain its integrity during excretion. Similar metabolic stability was observed for ⁶⁴Cu(DO2A-xy-TPP)⁺ (Figure SI).

The radioactivity detected in the urine and feces samples represents only the portion excreted from both renal and hepatobiliary routes. The remaining radioactivity is still “trapped” in organ tissues. We examined the stability of ⁶⁴Cu(DO3A-PEG₂-TPP) in the liver and found that there was no intact

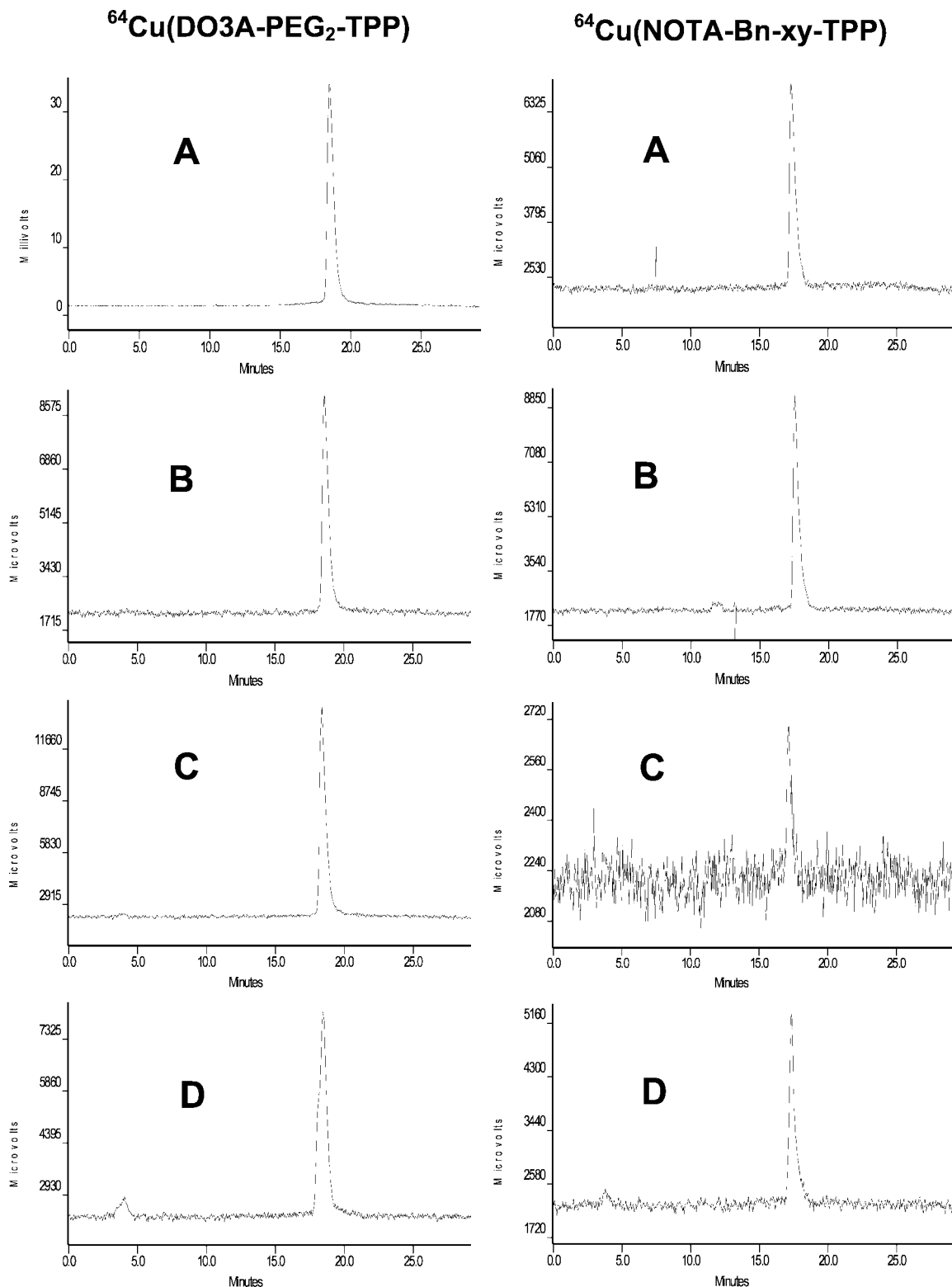


Figure 8. Radio-HPLC chromatograms of $^{64}\text{Cu}(\text{DO3A-PEG}_2\text{-TPP})$ (left) and $^{64}\text{Cu}(\text{DO3A-Bn-xy-TPP})$ (right) in saline before injection (A), in the urine at 30 min p.i. (B), in the urine at 120 min p.i. (C), and in the feces at 120 min p.i. (D). Each mouse was administered with $\sim 100 \mu\text{Ci}$ of the ^{64}Cu radiotracer.

$^{64}\text{Cu}(\text{DO3A-PEG}_2\text{-TPP})$ in the liver homogenate (Figure SII). While the identity of the two radiometric peaks at 5 and 10 min (Figure SII) is unclear at this moment, the HPLC chromatographic pattern of $^{64}\text{Cu}(\text{DO3A-PEG}_2\text{-TPP})$ in the liver homogenate is very similar to that of ^{64}Cu -labeled TETA-octreotide and that of ^{64}Cu -DOTA in the rat liver homogenate.^{51,52} On the basis of the literature data from the in vivo stability studies of ^{64}Cu complexes of tetraazamacrocycles,^{51–55} it is

reasonable to believe that the presence of two radiometric peaks at 5 and 10 min is most likely caused by transchelation of ^{64}Cu from $^{64}\text{Cu}(\text{DO3A-PEG}_2\text{-TPP})$ to superoxide dismutase (SOD), which is a homodimeric enzyme abundant in the liver and kidneys.⁵⁶

The metabolism of the ^{64}Cu -labeled biomolecules (antibodies and small peptides) and ^{64}Cu complexes of tetraazamacrocycles has been investigated extensively.^{51–64}

These studies clearly demonstrate that the kinetic inertness of the ⁶⁴Cu chelate is of particular importance for the in vivo stability of ⁶⁴Cu radiopharmaceuticals,⁵¹ and their instability is often caused by transchelation of ⁶⁴Cu from the ⁶⁴Cu-BFC chelate to the proteins in high concentrations, namely, SOD in the liver.^{51,56} For target-specific ⁶⁴Cu radiotracers, the tumor uptake is predominantly determined by receptor binding affinity of the targeting biomolecule (antibody or small peptide). Thus, the BFCs for ⁶⁴Cu chelation should be those that form the ⁶⁴Cu-BFC chelates with high kinetic inertness in order to minimize liver radioactivity accumulation. For the ⁶⁴Cu-labeled TPP cations as described in this study, however, the BFC contributes greatly to not only the radiotracer tumor uptake but also their excretion kinetics from noncancerous organs, such as liver and lungs. The BFCs for ⁶⁴Cu chelation should be those that result in the ⁶⁴Cu radiotracer with high tumor uptake and the best T/B, particularly tumor/heart and tumor/liver, ratios. From this point of view, both DO3A and DO2A are suitable as BFCs for ⁶⁴Cu-labeling of TPP cations. It must be noted that the radioactivity “trapped” inside the liver due to transchelation of ⁶⁴Cu is only a small portion of the injected radioactivity. Whenever possible, one has to consider the radioactivity excreted from renal and hepatobiliary routes (urine and feces samples), as well as the radioactivity “trapped” in various organ tissues.

Conclusion

In summary, we evaluated six new ⁶⁴Cu-labeled TPP cations for their biodistribution characteristics using athymic nude mice bearing U87MG glioma xenografts. We found that most of the new ⁶⁴Cu radiotracers have significant advantages over ^{99m}Tc-sestamibi with respect to their uptake in the heart and muscle. We also found that the TPP moieties, linkers, BFCs, and molecular charge have an effect on biological properties of ⁶⁴Cu-labeled TPP cations. For example, introduction of methoxy groups on the TPP cation improves the radiotracer clearance from the liver and lungs, but it also results in a significant washout from the tumor. Replacing xylene with the butylene linker results in a significant reduction of the tumor uptake, but the tumor/heart and tumor/lung ratios of the ⁶⁴Cu radiotracer remained relatively unchanged. Substitution of DO3A with NOTA-Bn has a significant adverse effect on tumor uptake of the ⁶⁴Cu radiotracer. Addition of an extra xy-TPP moiety in ⁶⁴Cu(DO2A-(xy-TPP)₂)²⁺ resulted in its dicationic character, high lipophilicity, higher liver uptake, and lower tumor uptake. Among the six ⁶⁴Cu radiotracers evaluated in this animal model, ⁶⁴Cu(DO2A-xy-TPP)⁺ is of particular interest due to its much lower liver uptake and better tumor/liver ratios than those of ⁶⁴Cu(DO3A-xy-TPP). On the basis of tumor uptake and tumor/heart and tumor/liver ratios of the ⁶⁴Cu radiotracers described in this study, we believe that both DO3A and DO2A are suitable BFCs for ⁶⁴Cu-labeling of TPP cations. ⁶⁴Cu(DO2A-xy-TPP)⁺ is the best candidate for more extensive evaluations in different tumor-bearing animal models.

Acknowledgment. The authors would like to thank Dr. Sulma I. Mohammed, the Director of Purdue Cancer Center Drug Discovery Shared Resource, Purdue University, for her assistance with the tumor-bearing animal model. This work is supported, in part, by research grants R01 CA115883 A2 (S.L.) from the National Cancer Institute (NCI), R21 EB003419-02 (S.L.) from the National Institute of Biomedical Imaging and Bioengineering (NIBIB), and R21 HL083961-01 from the National Heart, Lung, and Blood Institute (NHLBI).

Supporting Information Available: Detailed biodistribution data and T/B ratios for six new ⁶⁴Cu-labeled TPP cations are listed in Tables SI–SVI. Figure SI shows the radio-HPLC chromatograms of ⁶⁴Cu(DO2A-xy-TPP)⁺ in saline before injection (A) and in the urine at 30 min p.i. (B). Figure SII illustrates the radio-HPLC chromatogram of ⁶⁴Cu(DO3A-PEG₂-TPP) in the liver homogenate at 120 min p.i. These materials are available free of charge via the Internet at <http://pubs.acs.org>.

References

- (1) Kroemer, G.; Dallaporta, B.; Resche-Rigon, M. The mitochondrial death/life regulator in apoptosis and necrosis. *Annu. Rev. Physiol.* **1998**, *60*, 619–642.
- (2) Modica-Napolitano, J. S.; Aprille, J. R. Delocalized lipophilic cations selectively target the mitochondria of carcinoma cells. *Adv. Drug Delivery Rev.* **2001**, *49*, 63–70.
- (3) Duchen, M. R. Mitochondria in health and disease: perspectives on a new mitochondrial biology. *Mol. Aspects Med.* **2004**, *25*, 365–451.
- (4) Modica-Napolitano, J. S.; Singh, K. K. Mitochondria as targets for detection and treatment of cancer. Expert Reviews in Molecular Medicine, <http://www.ermm.cbuc.cam.ac.uk>, 2002, (02)00445-3a (short code: txt001ksb).
- (5) Johnson, L. V.; Walsh, M. L.; Chen, L. B. Localization of mitochondria in living cells with rhodamine 123. *Proc. Natl. Acad. Sci. U.S.A.* **1980**, *77*, 990–994.
- (6) Summerhayes, I. C.; Lampidis, T. J.; Bernal, S. D.; Nadakavukaren, J. J.; Nadakavukaren, K. K.; Shepard, E. L.; Chen, L. B. Unusual retention of rhodamine 123 by mitochondria in muscle and carcinoma cells. *Proc. Natl. Acad. Sci. U.S.A.* **1982**, *79*, 5292–5296.
- (7) Modica-Napolitano, J. S.; Aprille, J. R. Basis for the selective cytotoxicity of rhodamine 123. *Cancer Res.* **1987**, *47*, 4361–4365.
- (8) Davis, S.; Weiss, M. J.; Wong, J. R.; Lampidis, T. J.; Chen, L. B. Mitochondrial and plasma membrane potentials cause unusual accumulation and retention of rhodamine 123 by human breast adenocarcinoma-derived MCF-7 cells. *J. Biol. Chem.* **1985**, *260*, 3844–3850.
- (9) Dairkee, S. H.; Hackett, A. J. Differential retention of rhodamine 123 by breast carcinoma and normal human mammary tissue. *Breast Cancer Res. Treat.* **1991**, *18*, 57–61.
- (10) Gottlieb, E.; Thompson, C. B. Targeting the mitochondria to enhance tumor suppression. *Methods Mol. Biol.* **2003**, *223*, 543–554.
- (11) Mannella, C. A. The relevance of mitochondrial membrane topology to mitochondrial function. *Biochim. Biophys. Acta* **2006**, *1762*, 140–147.
- (12) Ross, M. F.; Kelso, G. F.; Blaikie, F. H.; James, A. M.; Cocheme, H. M.; Filipovska, A.; Da Ros, T. D.; Hurd, T. R.; Smith, R. A. J.; Murphy, M. P. Lipophilic triphenylphosphonium cations as tools in mitochondrial bioenergetics and free radical biology. *Biochem. (Moscow)* **2005**, *70*, 222–230.
- (13) Jakobs, S. High resolution imaging of live mitochondria. *Biochim. Biophys. Acta* **2006**, *1763*, 561–575.
- (14) Lichtshtein, D.; Kaback, H. R.; Blume, A. J. Use of a lipophilic cation for determination of membrane potential in neuroblastoma-glioma hybrid cell suspensions. *Proc. Natl. Acad. Sci. U.S.A.* **1979**, *76*, 650–654.
- (15) Hockings, P. D.; Rogers, P. J. The measurement of transmembrane electrical potential with lipophilic cations. *Biochim. Biophys. Acta* **1996**, *1282*, 101–106.
- (16) Huang, S. G. Development of a high throughput screening assay for mitochondrial membrane potential in living cells. *J. Biomol. Screening* **2002**, *7*, 383–389.
- (17) Herman, L. W.; Sharma, V.; Kronauge, J. F.; Barbarics, E.; Herman, L. A.; Piwnica-Worms, D. Novel hexakis(areneisonitrile)technetium(I) complexes as radioligands targeted to the multidrug resistance P-glycoprotein. *J. Med. Chem.* **1995**, *38*, 2955–2963.
- (18) Agrawal, M.; Abraham, J.; Balis, F. M.; Edgerly, M.; Stein, W. D.; Bates, S.; Fojo, T.; Chen, C. C. Increased ^{99m}Tc-Sestamibi accumulation in normal liver and drug resistant-tumors after the administration of the glycoprotein inhibitor, XR9576. *Clin. Cancer Res.* **2003**, *9*, 650–656.
- (19) Luker, G. D.; Fracasso, P. M.; Dobkin, J.; Piwnica-Worms, D. Modulation of the multidrug resistance P-glycoprotein: Detection with technetium-99m sestamibi in vivo. *J. Nucl. Med.* **1997**, *38*, 369–372.
- (20) Liu, Z. L.; Stevenson, G. D.; Barrett, H. H.; Kastis, G. A.; Bettan, M.; Furenid, L. R.; Wilson, D. W.; Woolfenden, J. M. Imaging recognition of multidrug resistance in human breast tumors using ^{99m}Tc-labeled monocationic agents and a high-resolution stationary SPECT system. *Nucl. Med. Biol.* **2004**, *31*, 53–65.
- (21) Liu, Z. L.; Stevenson, G. D.; Barrett, H. H.; Furenid, L. R.; Wilson, D. W.; Kastis, G. A.; Bettan, M.; Woolfenden, J. M. Imaging recognition of inhibition of multidrug resistance in human breast cancer

- xenografts using ^{99m}Tc -labeled sestamibi and tetrofosmin. *Nucl. Med. Biol.* **2005**, *32*, 573–583.
- (22) Muzzammil, T.; Ballinger, J. R.; Moore, M. J. ^{99m}Tc -sestamibi imaging of inhibition of the multidrug resistance transporter in a mouse xenografts model of human breast cancer. *Nucl. Med. Commun.* **1999**, *20*, 115–122.
- (23) Lorke, D. E.; Krüger, M.; Buchert, R.; Bohuslavizki, K. H.; Clausen, M.; Schumacher, U. In vitro and in vivo tracer characteristics of an established multidrug-resistant human colon cancer cell line. *J. Nucl. Med.* **2001**, *42*, 646–654.
- (24) Márián, T.; Balkay, L.; Szabó, G.; Krasznai, Z. T.; Hernádi, Z.; Galuska, L.; Szabó-Péli, J.; Ésik, O.; Trón, L.; Krasznai, Z. Biphasic accumulation kinetics of [^{99m}Tc]-hexakis-2-methoxyisobutyl isonitrile in tumour cells and its modulation by lipophilic P-glycoprotein ligands. *Eur. J. Pharm. Sci.* **2005**, *25*, 201–209.
- (25) Márián, T.; Szabó, G.; Goda, K.; Nagy, H.; Szincskák, N.; Juhász, I.; Galuska, L.; Balkay, L.; Mikecz, P.; Trón, L.; Krasznai, Z. In vivo and in vitro multitracer analysis of P-glycoprotein expression-related multidrug resistance. *Eur. J. Nucl. Med. Mol. Imaging* **2003**, *30*, 1147–1154.
- (26) Filippi, L.; Santoni, R.; Manni, C.; Danieli, R.; Floris, R.; Schillaci, O. Imaging primary brain tumor by single-photon emission computed tomography (SPECT) with technetium-99m Sestamibi (MIBI) and Tetrofosmin. *Curr. Med. Imaging Rev.* **2005**, *1*, 61–66.
- (27) Sharma, V.; Piwnica-Worms, D. Metal complexes for therapy and diagnosis of drug resistance. *Chem. Rev.* **1999**, *99*, 2545–2560.
- (28) Del Vecchio, S.; Salvatore, M. R. ^{99m}Tc -MIBI in the evaluation of breast cancer biology. *Eur. J. Nucl. Med. Mol. Imaging* **2004**, *31*, S88–S96.
- (29) Sharma, V. Radiopharmaceuticals for assessment of multidrug resistance P-glycoprotein-mediated drug transport activity. *Bioconjugate Chem.* **2004**, *15*, 1464–1474.
- (30) Vaidyanathan, G.; Zalutsky, M. R. Imaging drug resistance with radiolabeled molecules. *Curr. Pharm. Des.* **2004**, *10*, 2965–2979.
- (31) Sharma, V.; Piwnica-Worms, D. Monitoring multidrug resistance P-glycoprotein drug transport activity with single-photon emission computed tomography and positron emission tomography radiopharmaceuticals. *Top. Curr. Chem.* **2005**, *252* (Contrast Agents III), 155–178.
- (32) Krause, B. J.; Szabo, Z.; Becker, L. C.; Dannals, R. F.; Scheffel, U.; Seki, C.; Ravert, H. T.; Dipaola, A. F., Jr.; Wagner, H. N., Jr. Myocardial perfusion with [^{11}C] triphenyl phosphonium: measurements of the extraction fraction and myocardial uptake. *J. Nucl. Biol. Med.* **1994**, *38*, 521–526.
- (33) Madar, I.; Anderson, J. H.; Szabo, Z.; Scheffel, U.; Kao, P. F.; Ravert, H. T.; Dannals, R. F. Enhanced uptake of [^{11}C]TPMP in canine brain tumor: a PET study. *J. Nucl. Med.* **1999**, *40*, 1180–1185.
- (34) Madar, I.; Weiss, L.; Izbicki, G. Preferential accumulation of ^3H -tetraphenylphosphonium in non-small cell lung carcinoma in mice: comparison with ^{99m}Tc -MIBI. *J. Nucl. Med.* **2002**, *43*, 234–238.
- (35) Madar, I.; Ravert, H. T.; Du, Y.; Hilton, J.; Volokh, L.; Dannals, R. F.; Frost, J. J.; Hare, J. M. Characterization of uptake of the new PET imaging compound [^{18}F]fluorobenzyl triphenylphosphonium in dog myocardium. *J. Nucl. Med.* **2006**, *47*, 1359–1366.
- (36) Min, J. J.; Biswal, S.; Deroose, C.; Gambhir, S. S. Tetraphenylphosphonium as a novel molecular probe for imaging tumors. *J. Nucl. Med.* **2004**, *45*, 636–643.
- (37) Steichen, J. D.; Weiss, M. J.; Elmaleh, D. R.; Martuza, R. L. Enhanced in vitro uptake and retention of ^3H -tetraphenylphosphonium by nervous system tumor cells. *J. Neurosurg.* **1991**, *74*, 116–122.
- (38) Cheng, Z.; Winant, R. C.; Gambhir, S. S. A new strategy to screen molecular imaging probe uptake in cell culture without radiolabeling using matrix-assisted laser desorption/ionization time-of-flight mass spectrometry. *J. Nucl. Med.* **2005**, *46*, 878–886.
- (39) Wang, J.; Yang, C. T.; Kim, Y. S.; Sreerama, S. G.; Cao, Q.; Li, Z.; He, Z.; Chen, X.; Liu, S. ^{64}Cu -Labeled triphenylphosphonium and triphenylarsonium cations as highly tumor-selective PET imaging agents. *J. Med. Chem.* **2007**, *50*, 5057–5069.
- (40) Bähr, O.; Wick, W.; Weller, M. Modulation of MDR/MRP by wild-type and mutant p53. *J. Clin. Invest.* **2001**, *107*, 643–645.
- (41) Bähr, O.; Rieger, J.; Duffner, F.; Meyermann, R.; Weller, M.; Wick, W. P-glycoprotein and multidrug resistance-associated protein mediate specific patterns of multidrug resistance in malignant glioma cell lines, but not in primary glioma cells. *Brain Pathol.* **2003**, *13*, 482–494.
- (42) Le Jeune, N.; Perek, N.; Denoyer, D.; Dubois, F. Influence of glutathione depletion on plasma membrane cholesterol esterification and on Tc-99m-Sestamibi and Tc-99m-Tetrofosmin uptakes; a comparative study in sensitive U87MG and multidrug-resistant MRP1 human glioma cells. *Cancer Biother. Radiopharm.* **2004**, *19*, 411–421.
- (43) Nakatsu, S.; Kondo, S.; Kondo, Y.; Yin, D.; Peterson, J. W.; Kaakaji, R.; Morimura, T.; Kikuchi, H.; Takeuchi, J.; Barnett, G. H. Induction of apoptosis in multi-drug resistant (MDR) human glioblastoma cells by SN38, a metabolite of the camptothecin derivative CPT-11. *Cancer Chemother. Pharmacol.* **1997**, *39*, 417–423.
- (44) Kumar, K.; Tweedle, M. F.; Malley, M. F.; Gougoutas, J. Z. Synthesis, stability, and crystal structure studies of some Ca^{2+} , Cu^{2+} , and Zn^{2+} complexes of macrocyclic polyamino carboxylates. *Inorg. Chem.* **1995**, *34*, 6472–6480.
- (45) Anderson, C. J.; Green, M. A.; Fujibayashi, Y. Chemistry of copper radionuclides and radiopharmaceutical products. *Handbook Radiopharm.* **2003**, *401*, 422.
- (46) Blower, P. J.; Lewis, J. S.; Zweit, J. Copper radionuclides and radiopharmaceuticals in nuclear medicine. *Nucl. Med. Biol.* **1996**, *23*, 957–980.
- (47) Smith, S. V. Molecular imaging with copper-64. *J. Inorg. Biochem.* **2004**, *98*, 1874–1901.
- (48) Reichert, D. E.; Lewis, J. S.; Anderson, C. J. Metal complexes as diagnostic tools. *Coord. Chem. Rev.* **1999**, *184*, 3–66.
- (49) Liu, S. The role of coordination chemistry in development of target-specific radiopharmaceuticals. *Chem. Soc. Rev.* **2004**, *33*, 1–18.
- (50) Liu, S. Bifunctional coupling agents for target-specific delivery of metallic radionuclides. *Adv. Drug Delivery Rev.*, accepted.
- (51) Bass, L. A.; Wang, M.; Welch, M. J.; Anderson, C. J. In vivo transchelation of copper-64 from TETA-Octreotide to superoxide dismutase in rat liver. *Bioconjugate Chem.* **2000**, *11*, 527–532.
- (52) Boswell, C. A.; Sun, X.; Niu, W.; Weisman, G. R.; Wong, E. H.; Rheingold, A. L.; Anderson, C. J. Comparative in vivo stability of copper-64-labeled cross-bridged and conventional tetraazamacrocyclic complexes. *J. Med. Chem.* **2004**, *47*, 1465–1474.
- (53) Boswell, C. A.; McQuade, P.; Weisman, G. R.; Wong, E. H.; Anderson, C. J. Optimization of labeling and metabolite analysis of copper-64-labeled azamacrocyclic chelators by radio-LC-MS. *Nucl. Med. Biol.* **2005**, *32*, 29–38.
- (54) Anderson, C. J. Metabolism of radiometal labeled proteins and peptides: what are the real radiopharmaceuticals in vivo. *Cancer Biother. Radiopharm.* **2001**, *16*, 451–455.
- (55) Sprague, J. E.; Peng, Y.; Fiamengo, A. L.; Woodin, K. S.; Southwick, E. A.; Wiseman, G. R.; Wong, E. H.; Golden, J. A.; Rhengold, A. L.; Anderson, C. J. Synthesis, characterization and in vivo studies of Cu(II)-64-labeled cross-bridged tetraazamacrocyclic-amide complexes as models of peptide conjugate imaging agents. *J. Med. Chem.* **2007**, *50*, 2527–2535.
- (56) Bartnikas, T. B.; Gitlin, J. D. Mechanisms of biosynthesis of the mammalian copper/zinc superoxide dismutase. *J. Biol. Chem.* **2003**, *278*, 33602–33608.
- (57) Deshpande, S. V.; DeNardo, S. J.; Meares, C. F.; McCall, M. J.; Adams, J. P.; Moi, M. K.; DeNardo, G. L. Copper-67-labeled monoclonal antibody Lym-1, a potential radiopharmaceutical for cancer therapy: Labeling and biodistribution in RAJI tumored mice. *J. Nucl. Med.* **1988**, *29*, 217–225.
- (58) Li, W. P.; Lewis, J. S.; Kim, J.; Bugaj, J. E.; Johnson, M. A.; Erion, J. L.; Anderson, C. J. DOTA-D-Tyr¹-Octreotate: a somatostatin analogue for labeling with metal and halogen radionuclides for cancer imaging and therapy. *Bioconjugate Chem.* **2002**, *13*, 721–728.
- (59) McQuade, P.; Miao, Y.; Yoo, J.; Quinn, T. P.; Welch, M. J.; Lewis, J. S. Imaging of melanoma using ^{64}Cu - and ^{86}Y -DOTA-ReCCM-SH(Arg¹¹), a cyclized peptide analogue of α -MSH. *J. Med. Chem.* **2005**, *48*, 2985–2992.
- (60) Biddlecombe, G. B.; Rogers, B. E.; de Visser, M.; Parry, J. J.; de Jong, M.; Erion, J. L.; Lewis, J. S. Molecular imaging of gastrin-releasing peptide receptor-positive tumors in mice using ^{64}Cu - and ^{86}Y -DOTA-(Pro¹, Tyr⁴)-Bombesin(1–14). *Bioconjugate Chem.* **2007**, *18*, 724–730.
- (61) Parry, J. J.; Andrews, R.; Rogers, B. E. MicroPET imaging of breast cancer using radiolabeled bombesin analogs targeting the gastrin-releasing peptide receptor. *Breast. Cancer Res. Treat.* **2007**, *101*, 175–183.
- (62) Parry, J. J.; Kelly, T. S.; Andrews, R.; Rogers, B. E. In vitro and in vivo evaluation of ^{64}Cu -labeled DOTA-Linker-Bombesin(7–14) analogues containing different amino acid linker moiety. *Bioconjugate Chem.* **2007**, *18*, 1110–1117.
- (63) Chen, X.; Liu, S.; Hou, Y.; M.; Tohme, M.; Park, R.; Bading, J. R.; Conti, P. S. MicroPET imaging of breast cancer α_v -integrin expression with ^{64}Cu -labeled dimeric RGD peptides. *Mol. Imaging Biol.* **2005**, *6*, 350–359.
- (64) Wu, Y.; Zhang, X.; Xiong, Z.; Cheng, Z.; Fisher, D. R.; Liu, S.; Gambhir, S. S.; Chen, X. MicroPET imaging of glioma $\alpha_v\beta_3$ integrin expression using ^{64}Cu -labeled tetrameric RGD peptide. *J. Nucl. Med.* **2005**, *46*, 1707–1718.